PERFORMANCE ANALYSIS OF SUSPENSION MANUAL WHEELCHAIRS

by

Andrew Michael Kwarciak

BS, Bioengineering, Arizona State University, 2001

Submitted to the Graduate Faculty of

the School of Engineering in partial fulfillment

of the requirements for the degree of

Master of Science in Bioengineering

University of Pittsburgh

2003

UNIVERSITY OF PITTSBURGH

SCHOOL OF ENGINEERING

This thesis was presented

by

Andrew Michael Kwarciak

It was defended on

December 3, 2003

and approved by

Michael L. Boninger, M.D., Departments of Physical Medicine and Rehabilitation and Bioengineering

Dan Ding, Ph.D., Department of Rehabilitation Science and Technology

Thesis Director: Rory A. Cooper, Ph.D., Departments of Rehabilitation Science and Technology and Bioengineering

PERFORMANCE ANALYSIS OF SUSPENSION MANUAL WHEELCHAIRS

Andrew Michael Kwarciak, MS

University of Pittsburgh, 2003

Throughout the course of daily activities, wheelchair users are subjected to a variety of whole-body vibrations that are suspected to cause a number of harmful physiological effects. In efforts to improve rider comfort and prevent secondary injuries, manufacturers of manual wheelchairs have integrated suspension systems into their designs. The purpose of this research was to provide a thorough evaluation of currently available suspension manual wheelchairs and to determine the advantages, if any, of wheelchair suspension.

The evaluation was composed of two sections: 1) a durability and cost analysis of three selected suspension manual wheelchairs; and 2) a pair of functional tests comparing suspension manual wheelchairs to standard folding- and rigid-frame models. The durability and cost analysis revealed that integrated suspension did not significantly improve wheelchair fatigue life; in fact, some modifications reduced wheelchair integrity. In addition, their increased expense considerably lowered their value in relation to the other types of wheelchairs. Altogether, little evidence was found to suggest that suspension manual wheelchairs provide advantages in terms of durability or value over non-suspension, folding-frame wheelchairs.

Functional testing was used to evaluate the ability of suspension manual wheelchairs to reduce the transmission of vibrations to the rider during various height curb descents and while traversing a level, uneven surface. In addition, impact force was measured during curb descent trials and used in the comparison. The results suggest that while the suspension manual wheelchairs provided significant ($p = .0002$) reduction in seat accelerations over both types of standard wheelchairs, this was due to the superiority of one wheelchair, the Sunrise Medical Quickie XTR. Furthermore, few significant improvements were found in terms of impact force and vibration dose value, which was calculated from seat accelerations measured during uneven surface testing. Overall the results indicate that suspension manual wheelchairs are not suited to suppress the shock vibrations or repeated low-level vibrations generated by curb descents and uneven terrain, respectively.

The results of this research should be used to develop a more adequate wheelchair suspension system, and more importantly, should be considered by clinicians and wheelchair users when selecting a wheelchair for everyday use.

TABLE OF CONTENTS

LIST OF TABLES

LIST OF FIGURES

ACKNOWLEDGEMENTS

I would like to thank the faculty and staff of the Human Engineering Research Laboratories for their continual support, especially my mentor Dr. Rory Cooper. Without Dr. Cooper's guidance and seemingly endless participation in data collection, this research would not have been possible. I would like to thank Drs. Michael Boninger, Shirley Fitzgerald, Dan Ding, and Guo Song Feng for helping me bring my efforts to fruition. I would also like to thank William Ammer, John Duncan, Beth Ann Kaminski, Stephanie Martin, and Erik Wolf and everyone who provided assistance with data collection as well as Michael Dvorsnak and Erik Wolf and for their assistance with data analysis. And finally, I want to thank my family and my fiancée, Karen, for their endless encouragement and confidence, this one is for you.

1.0 INTRODUCTION

Much research has been performed on whole-body vibrations (WBV) and their potentially damaging effects on the human body; and though no definitive relationship exists, the development of low back pain and secondary injury in persons exposed to WBV has been well documented and evaluated.[1-5] Recent studies have attempted to more accurately categorize the possible mechanisms of injury related to WBV[6-11] as well as develop models that may be used to optimize preventive measures.[12-15] Although none of this research addresses the effects of WBV on subjects with a spinal cord injury, the conclusions drawn from previous studies have influenced approaches to wheelchair, and wheelchair component, design.

Wheelchair use presents one of the greatest risks of low back pain and injury due to associated WBV exposure. In terms of vibration transmission, the most vulnerable position of the body is the seated position;[1] and for those who rely on wheelchairs as their primary means of mobility, this position may be assumed for up to 14 hours a day (derived from a study by Hoover et al[16]). During this time wheelchair users are subjected to a variety of repeated low-level vibrations as well as infrequent, high magnitude shock vibrations.[17] More importantly, it is evident that most of the energy from these vibrations is absorbed by the rider.[17] This poses a considerable threat to the health and comfort of wheelchair users considering that repeated exposure to WBV has been shown to compromise the ability of the spine and back muscles to absorb and distribute suddenly

applied loads.[3,18] With regards to wheelchair use, these type of loads can be experienced during common tasks such as transfers and wheelchair transportation. Furthermore, VanSickle et al[19] reported that wheelchair propulsion produces vibration loads that exceed ISO 2631-1 standards[20] at the seat of the wheelchair and the head of the user. Suppression of these vibrations may be accomplished through postural[9,11] or seating adaptations;[21,22] however these approaches are not optimized and are not sufficient for shock vibration absorption.

The need to address the potential danger posed by extensive WBV exposure, especially to shock vibrations, has motivated the development of better-adapted wheelchairs. In efforts to prevent secondary injuries, manufacturers of manual wheelchairs have integrated suspension systems into their designs. By positioning suspension elements between the axle and the seat, they have intended to reduce the transmission of injurious vibrations to the user.

Several approaches to wheelchair suspension have been introduced, each offering a different type and configuration of the suspension element. So far three types of suspension elements are most common: elastomers, springs, and spring and damper units. Elastomers are natural rubber or rubber-like materials that exhibit linear viscoelastic behavior and provide internal damping, which increases with the frequency of vibration.[23] Metal springs ideally exhibit linear load-deflection curves, as governed by Hooke's Law, and provide effective shock and vibration control; however, they transmit high-frequency vibrations and offer little damping.[23] The spring and damper unit is a combination device capable of reducing shock vibrations and their resulting oscillations. Of equal importance to the type of suspension element, is its configuration on the wheelchair. This varies notably between wheelchairs depending on manufacturer preference and

on the specific design and intended function of the wheelchair. Each of the four suspension manual wheelchairs included in this research presents a unique combination of suspension element and suspension configuration, and therefore, potentially unique capabilities.

The purpose of this research was to provide a thorough evaluation of currently available suspension manual wheelchairs and to determine the advantages, if any, of wheelchair suspension. The evaluation was composed of two sections: 1) a durability and cost analysis of three selected suspension manual wheelchairs; and 2) a pair of functional tests comparing suspension manual wheelchairs to standard folding- and rigid-frame models. Durability and value were determined using the results obtained from a series of standardized fatigue tests. Functional testing involved measuring the vibration transmission of all three types of wheelchairs during curb descents and while traversing uneven terrain. In addition, impact forces were measured and compared for the curb descents. Together the studies provided a quantitative measure of the reliability of suspension manual wheelchairs. Further testing is needed to obtain a better appreciation for how suspension manual wheelchairs affect users; however the results presented here can be used to assist clinicians and wheelchair users in the selection of a wheelchair for daily use as well as in the future development of manual wheelchair suspension.

2.0 FATIGUE TESTING OF SUSPENSION MANUAL WHEELCHAIRS

Suspension manual wheelchairs are targeted to active, experienced users who are expected to place a high amount of stress on their wheelchairs during daily activities. Novice users are often ill suited for such wheelchairs because integrated suspension tends to limit adjustability and may reduce stability. In this respect, suspension manual wheelchairs have a more focused consumer base. To comply with the needs of this experienced group of intended users, suspension manual wheelchairs must demonstrate an acceptable level of durability.

To assess the structural integrity of wheelchairs, the American National Standards Organization (ANSI) in cooperation with the Rehabilitation Engineering and Assistive Technology Society of North America (RESNA) has developed a set of testing standards, consistent with those created by the International Organization for Standardization (ISO).[24] Section 8 of these standards includes two fatigue tests: the double-drum test and the curb-drop test. These two tests, when performed in succession, simulate 3-5 years of use by an active individual.[25]

Previous studies have used these fatigue tests to evaluate the durability of standard manual wheelchairs.[26,27,28] Cooper et al[26] reported that ultra lightweight wheelchairs have a significantly longer fatigue life than lightweight wheelchairs, which in turn, have a longer fatigue life than depot wheelchairs. In addition, ultra lightweight wheelchairs are the most cost effective over the life of the wheelchair, costing 3.4 times less (dollars per life cycle) than depot wheelchairs and

2.3 times less (dollars per life cycle) than the lightweight wheelchairs. A subsequent study, conducted by Fitzgerald et al,[27] used ANSI/RESNA fatigue tests to evaluate and compare 61 manual wheelchairs. The study revealed that many wheelchairs were not compliant with ISO requirements and confirmed that ultra lightweight wheelchairs survived significantly longer than lightweight and depot wheelchairs.

The fatigue life of the common suspension manual wheelchair is unknown. Despite this lack of knowledge, these wheelchairs are regularly provided for active users. The purpose of this study was to use ANSI/RESNA fatigue tests to determine the durability and value of three common suspension manual wheelchair designs and to compare the results with those previously obtained from lightweight and ultra lightweight wheelchairs. Ultra lightweight wheelchairs offer comparable adjustability and maneuverability, and similar to suspension manual wheelchairs, they are designed to provide long-term mobility for active users. Alternatively, lightweight wheelchairs offer minimal adjustability and are less durable; however, they typically cost less and therefore may provide better value. For this study it was hypothesized that: (1) the total number of equivalent cycles for each of the three suspension wheelchairs would not be significantly different; (2) the inclusion of suspension elements would significantly increase the total number of equivalent cycles over both lightweight and ultra lightweight wheelchairs; and (3) the equivalent cycles per dollar for the suspension wheelchairs would be significantly higher than that for both lightweight and ultra lightweight wheelchairs.

2.1 METHODS

A total of nine suspension manual wheelchairs, three from each manufacturer (Figure 1), were used in this study. The cost of each wheelchair was: $2,475 (Invacare A-6S[a]); $3,087 (Permobil Colours Boing[b]); and $2,325 (Sunrise Medical Quickie XTR[c]). Each wheelchair represents the base model that was purchased anonymously from the manufacturers. Prior to testing, each wheelchair was measured and adjusted (where applicable) to meet similar critical dimensions (Table 1) and fitted with factory issued rear wheels and casters. All rear tires were inflated to their rated pressure and verified with a calibrated gauge. For the following tests, a 100 kg (220 lbs) ANSI/RESNA wheelchair test dummy was secured in each wheelchair.[24]

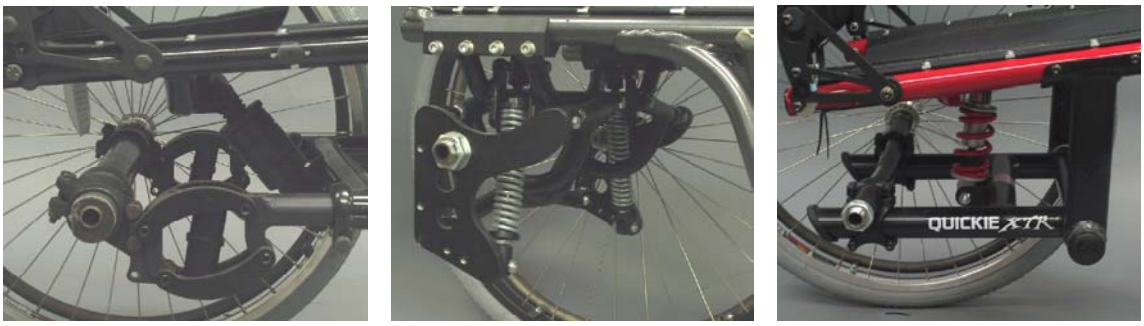

Figure 1. Three suspension manual wheelchairs used in this study: Invacare A-6S (left), Colours Boing (middle), and Sunrise Medical Quickie XTR (right).

The first test performed in the series was the double-drum test (DDT). The DDT consists of two metal cylindrical drums (200 mm diameter), each fitted with two 12 mm slats positioned 180° apart (Figure 2). The slats are designed to simulate vibrations experienced by traversing such obstacles as door thresholds and sidewalk cracks. During testing, the drums are rotated at a constant surface velocity of 1 m/s. The front drum is rotated 5-7% faster than the rear drum to avoid harmonic vibration patterns. A swing-arm is attached to the wheelchair to keep it balanced

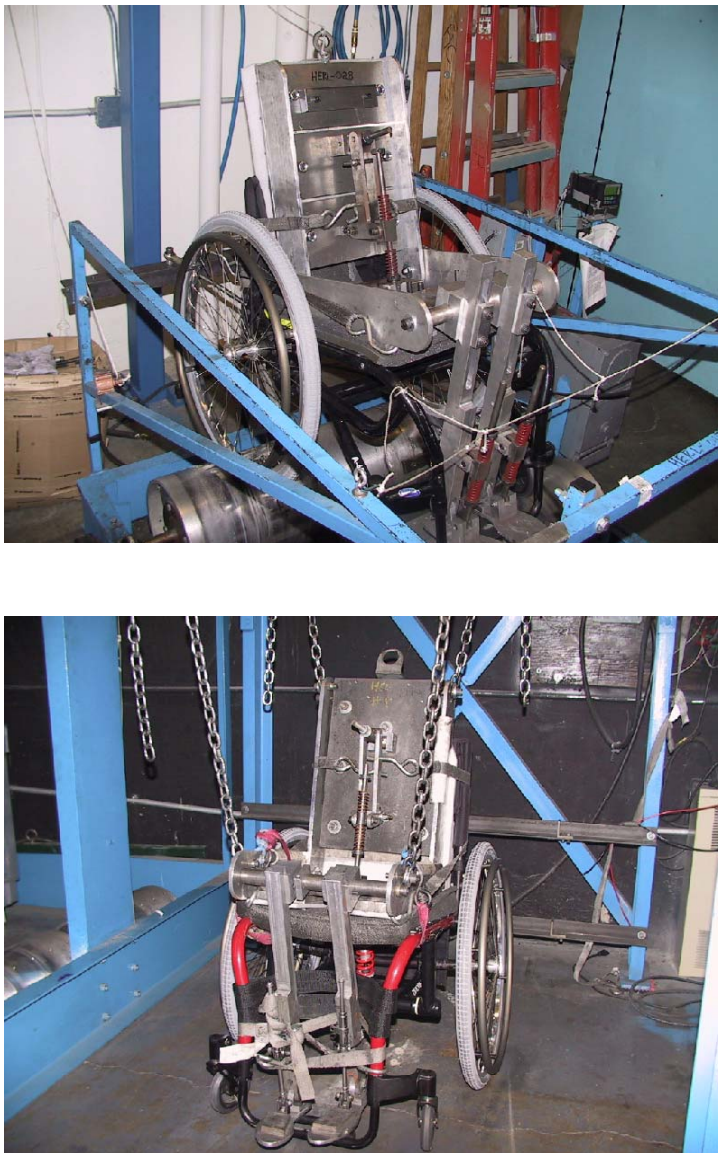

Figure 2. ANSI/RESNA fatigue tests: the double-drum test (top) and the curb-drop test (bottom).

over the drums. One full revolution of the rear roller is defined as a single cycle on the DDT. The second test, the curb-drop test (CDT), is designed to simulate forces sustained during curb descents. The CDT lifts the wheelchair 5 cm then allows it to drop onto a concrete floor (Figure 2). The height is calibrated and checked throughout the course of testing.

Table 1: Manufacturer, Model, and Critical Dimensions for Wheelchairs Tested

Manufacturer/ Model	Seat Angle (°)	Seat Depth (mm)	Seat Width (mm)	Seat Height (mm)	Backrest Angle (°)	Backrest Height (mm)	Backrest Width (mm)	Wheelbase (mm)
Invacare								
A-6S 1	9	406	405	437	8	320	410	421
A-6S 2	13	407	407	442	9	325	412	417
A-6S 3	11	407	405	440	8	320	413	421
Permobil								
Colours Boing 1	7	408	394	468	10	380	405	423
Colours Boing 2	11	407	395	464	7	383	406	429
Colours Boing 3	11	410	393	468	5	380	406	444
Sunrise Medical								
Quickie XTR 1	13	406	394	465	9	431	423	393
Quickie XTR 2	12	405	393	464	7	431	424	384
Quickie XTR 3	11	407	394	467	7	432	421	400

Each wheelchair was first to be tested on the DDT for 200,000 cycles. Upon completion, each wheelchair was inspected for incidences of catastrophic failure, which is defined as any permanent damage or deformation that impairs the operability or safety of the wheelchair. If cleared of such failures, the wheelchair was transferred to the CDT and run for 6,666 drops. Successful completion of one full set of the DDT and CDT is required to meet ISO standards. For this study, the sequence of tests was repeated until failure. All wheelchairs were inspected at least every 10,000 double-drum cycles and 300 curb-drops and testing logs were kept to record progress and note any problems. The double-drum and curb drops cycles chosen for these tests are those described in ISO 7176-8.[29]

As a means of comparing performance and value, the equivalent number of cycles completed by each model were calculated, using the following equation:

Equivalent Cycles = (Double-Drum Test Cycles) + 30 • (Curb-Drop Test Drops)

This equation is based upon the ratio for DDT cycles and CDT drops in section 8 of the ANSI/RESNA Wheelchair Standards. In order to determine relative operational cost per equivalent test cycle, the total number of equivalent cycles completed was divided by the initial purchase price. This yields a parameter that we refer to as value, which has units of equivalent cycles per dollar. The value is an estimate of life-cycle costs for each wheelchair's useful life span. Maintenance costs were not used in determining value, since minimal maintenance costs were incurred during this study. All methods of fatigue testing and analysis were consistent with those used in preceding studies on wheelchair performance.[26,27,28]

The durability and value of the suspension wheelchairs were compared with those of lightweight and ultra lightweight folding-frame wheelchairs, previously reported by Cooper et al.[26,28] The lightweight wheelchairs included three of each of the following models: Everest & Jennings EZ Lite, Invacare Rolls 2000, and Sunrise Medical Quickie Breezy. The ultra lightweight wheelchairs tested in the latter study included four of each of the following models: Invacare Action XTRA, Kuschall Champion 1000, Everest & Jennings Vision Epic, and Sunrise Medical Quickie II. The critical dimensions of the suspension wheelchairs tested as part of this study were specified from the manufacturers to be comparable to those of both the lightweight and ultra lightweight wheelchairs.

All nine suspension wheelchairs were tested according to a balanced randomization. Analysis of variance (ANOVA) was used to identify significant differences, in total number of equivalent cycles and value, between the three different types of suspension wheelchairs. Based on the same two factors, comparisons between suspension wheelchairs and both ultra lightweight and lightweight wheelchairs were made using independent t-tests for equality of means (equal variances not assumed) and ANOVA. The Bonferroni post-hoc analysis[30] was used to identify significant interactions of individual wheelchairs. All analyses were performed using SPSS[d] with a significance level of .05.

2.2 RESULTS

The total number of cycles completed by each wheelchair on the DDT and CDT are presented in table 2. Of the nine wheelchairs tested, six passed ISO fatigue standards. All of the Colours Boing wheelchairs experienced similar caster failures (Figure 3) during the initial DDT. The first wheelchair tested, the Boing 2, was initially run on the DDT with the original equipment manufacturer, low-durometer polyurethane casters. After about 31,000 cycles it was noticed that the caster tires were shredding off their plastics rims and testing was stopped. Replacement caster wheels were obtained from the manufacturer; however, these wheels had tires made from high-durometer polyurethane.

Table 2: Double-drum and Curb-drop Test Results for Selected Suspension Manual Wheelchairs

Manufacturer/ Model	Double-Drum Cycles	Curb-Drop Cycles	Total Equivalent Cycles	Location of Failure
Invacare				
A-6S 1	400,000	13,332	799,960	Frame, right telescoping tube
A-6S 2	207,335	6,666	407,315	Frame, left seat along screw hole
A-6S 3	385,467	6,666	585,447	Frame right telescoping tube
Permobil				
Colours Boing 1	30,008	0	30,008	Right caster stem
Colours Boing 2	78,935	0	78,935	Left caster stem, right caster axle
Colours Boing 3	50,091	0	50,091	Right caster stem
Sunrise Medical				
Quickie XTR 1	1,000,000	33,330	2,000,000	Frame, seat shock mount
Quickie XTR 2	445,288	13,332	845,248	Frame, right seat along screw hole
Quickie XTR 3	430,532	13,332	830,492	Right caster mount

Figure 3. Example of the caster failures common to all Colours Boing models. This picture shows the failure of the right caster of Boing 3 on the initial double-drum test.

The new wheels were fitted to the caster forks and testing was resumed. After 78,935 cycles, testing of Boing 2 was ended after the fracture of the right caster stem and plastic deformation of the left caster axle were detected. Prior to testing the remaining two Colours wheelchairs, the original caster wheels were replaced with the high-durometer caster wheels. Boing 1 was run for 30,008 cycles before testing was ended due to permanent deformation of the right caster stem.

Boing 3 was run for 50,091 cycles before a similar failure of the right caster stem was noticed. Due to the failures of the caster stems during the initial DDT, no CDT cycles were tested, and consequently, all three wheelchairs failed to meet ISO standards.

Conversely all of the Invacare A-6S wheelchairs completed at least one full set of DDT and CDT tests. The first wheelchair, A-6S 1, was tested in its initial configuration with the factory standard elastomers. During the second set of tests, it was realized that the prescribed weight capacity of the elastomers (180 lbs) was unfit to support the weight of the test dummy (220 lbs). New elastomers, with an appropriate weight range (221-250 lbs), were ordered and installed on each of the three A-6S models. Testing of A-6S 1 continued until the fracture of the right telescoping tube (Figure 4) was found after completion of the second CDT. This proved to be the longest survival of any A-6S wheelchair. A-6S 2 experienced a fracture along the seat

Figure 4. Fracture of the right telescoping tube of the Invacare A-6S 1. The A-6S 3 experienced a similar failure of the right telescoping tube.

section of the frame (Figure 5) after 207,000 DDT cycles and 6,666 CDT drops and A-6S 3 experienced a fracture of the right telescoping tube, similar to that of A-6S 1, after 385,000 DDT cycles and 6,666 CDT drops. All A-6S wheelchairs passed ISO 7176-08 standards.

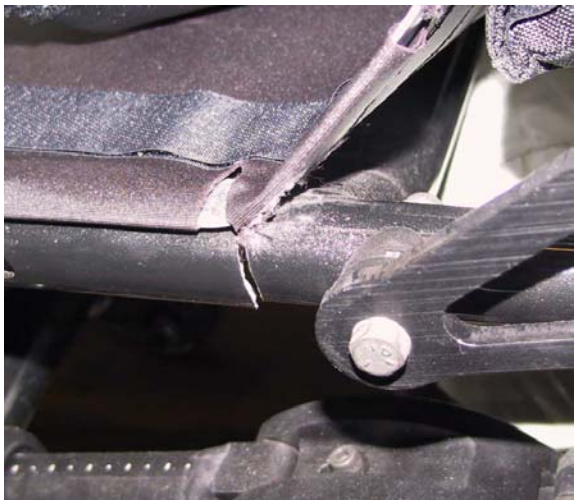

Figure 5. Fracture of the left seat section of the frame on the Invacare A-6S 2. This same type of failure occurred on the Quickie XTR 2.

Of all three wheelchair types, the Quickie XTR demonstrated the greatest durability. All three XTR models outlasted every other wheelchair tested, with the XTR 1 demonstrating the longest lifetime, completing 1,000,000 DDT cycles and about 33,330 CDT drops before experiencing a fracture in the seat shock mount (Figure 6). XTR 2 and XTR 3 had similar lifetimes, each completing two full sets of tests before failing on the third DDT. XTR 2 lasted for about 445,000 DDT cycles before experiencing a fracture in the right seat of the frame. XTR 3 lasted for about 430,000 DDT cycles before experiencing a fracture of the right caster mount (Figure 7). Analysis of variance revealed significant differences ($p = .033$) in the number of equivalent cycles among the suspension wheelchairs tested. A Bonferroni post-hoc analysis showed that the

Quickie XTR significantly (p = .036) outlasted the Colours Boing. No other significant differences in equivalent cycles were found.

Figure 6. Fracture of the seat shock frame support on the Quickie XTR 1.

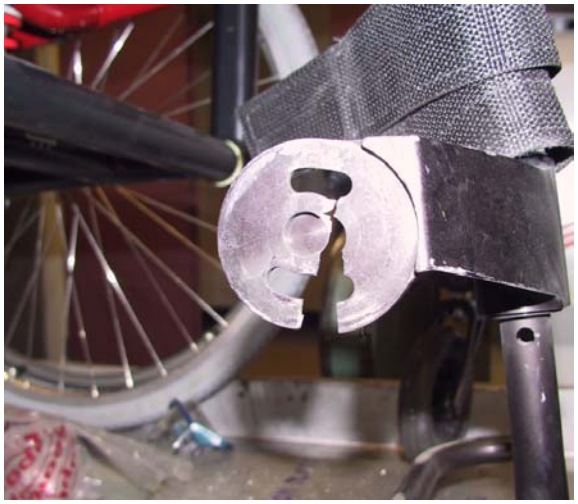

Figure 7. Fracture of the right caster mount of the Quickie XTR 3.

Figure 8 presents the results of the cost analysis for the wheelchairs compared in this study. The value assigned to each wheelchair represents the mean value of all wheelchairs of that particular

model. Analysis of variance revealed significant differences ($p = .031$) in value among the suspension wheelchairs. Of the three suspension wheelchairs, the Quickie XTR demonstrated the highest value (527 equivalent cycles per dollar). This value is about 31 times higher than the value of the Colours Boing and about 2.2 times higher than the value of the Invacare A-6S. A Bonferroni post hoc analysis showed significant difference in value ($p = .034$) between the Quickie XTR and the Colours Boing. The Colours Boing demonstrated the lowest value of all wheelchairs tested (17 equivalent cycles per dollar).

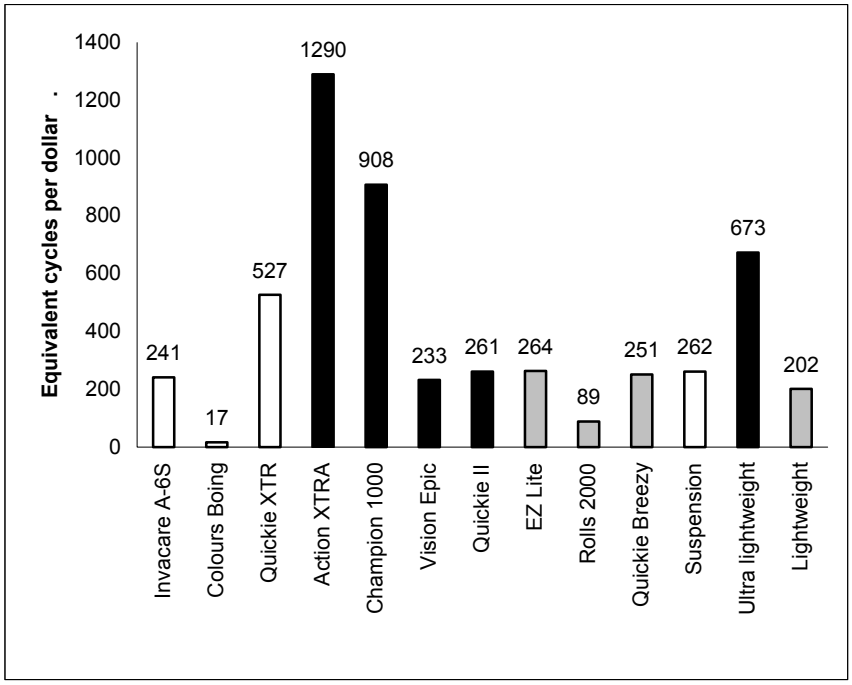

Figure 8. Mean value (equivalent cycles per dollar) of each wheelchair. White bars represent the suspension wheelchairs; black bars represent the ultra lightweight wheelchairs; gray bars represent the lightweight wheelchairs. The last three bars represent the average values for each wheelchair type.

The results from the suspension wheelchairs tested in this study were compared to the results for four different ultra lightweight folding-frame wheelchair models (twelve wheelchairs total), reported in a previous study.[26] An independent t-test for equality of means revealed no

significant differences ($p = .138$) between the number of equivalent cycles completed by the suspension and ultra lightweight wheelchairs. The suspension wheelchairs averaged about 625,266 ± 616,783 equivalent cycles, whereas the ultra lightweight wheelchairs averaged about 1,092,441 ± 730,624 equivalent cycles. Analysis of variance indicated significant differences ($p = .000$) amongst individual wheelchairs within each group. Of the seven different models, the Kuschall Champion 1000 completed the most average equivalent cycles (1,830,026), whereas the Colours Boing completed the fewest (53,011). A Bonferroni post hoc analysis showed significant differences between the Invacare Action XTRA and the Colours Boing and between the Champion 1000 and both the Colours Boing and the Invacare A-6S. No suspension wheelchair demonstrated significant improvement in durability over any of the ultra lightweight wheelchairs tested.

When value was compared amongst the wheelchairs, analysis of variance revealed significant differences ($p = .000$) between individual suspension and ultra lightweight wheelchairs. The suspension wheelchairs had a mean value of 262 equivalent cycles per dollar compared to 673 equivalent cycles per dollar for the ultra lightweight wheelchairs. A Bonferroni post-hoc analysis showed significant differences ($p \leq .05$) between the Champion 1000 and the Invacare A-6S and Colours Boing and between the Action XTRA and all three suspension wheelchairs.

Based on the lack of significance found between the suspension wheelchairs and the ultra lightweight wheelchairs, a similar comparison was made between the suspension wheelchairs and a group of previously tested lightweight wheelchairs.[28] As with the previous comparison, an independent t-test revealed no significant differences ($p = .069$) between the number of

equivalent cycles completed by the suspension and lightweight wheelchairs. The lightweight wheelchairs averaged about 187,326 ± 153,055 equivalent cycles, 437,940 cycles less than the suspension wheelchairs. Though the difference was not reflected in the t-test, an analysis of variance did reveal significant differences ($p = .004$) amongst individual wheelchairs within each group. With the exception of the Colours Boing wheelchairs, which posted the lowest number of equivalent cycles, the lightweight wheelchairs had lower totals than the suspension wheelchairs. The average number of equivalent cycles for each lightweight wheelchair was: E&J EZ Lite (240,166), Invacare Rolls 2000 (89,358), and Sunrise Medical Quickie Breezy (232,453). A Bonferroni post hoc analysis revealed significant differences between the Quickie XTR and all three lightweight wheelchairs.

In a comparison of value, analysis of variance revealed significant differences ($p = .047$) between the suspension and lightweight wheelchairs. The lightweight wheelchairs had a mean value of 202 equivalent cycles per dollar, 60 cycles per dollar lower than the value of the suspension wheelchairs. A Bonferroni post-hoc analysis showed significant differences ($p \leq .05$) between the Quickie XTR and the Invacare Rolls 2000.

2.3 DISCUSSION

The results reveal differences among the suspension wheelchairs and between the suspension wheelchairs tested and common ultra lightweight and lightweight folding-frame wheelchairs. Of the suspension wheelchairs, the Quickie XTR wheelchairs demonstrated the best durability and

the best value, both of which were significantly better than those demonstrated by the Colours Boing wheelchairs. These significant differences were primarily due to the poor performance of the latter group. It is suspected that the premature failures of the caster stems resulted from their quick-release design. Similar to quick-release rear wheel axles, the caster stems are hollow, in order to house a spring-loaded locking system. The design makes them easy to remove; unfortunately, it also reduces their load bearing capability. Further weakening the design was the exposure of the threaded section of each stem, which generated an additional stress concentration. During double-drum testing, the hollow axles were unable to withstand the force applied by the slats and thus became the locations of failure in all three wheelchairs.

In terms of value, the Colours Boing wheelchairs were the lowest among the wheelchairs tested in this study. This was due to their failure to complete the first set of DDT testing, which drastically affected the total number of equivalent cycles, and their higher cost ($3,087). Of the three suspension wheelchairs, the Colours Boing was the most expensive: about 1.25 times more than the cost of the Invacare A-6S and about 1.33 times more than the cost of the Quickie XTR. This elevated cost is most likely attributable to its complex a-arm suspension system, which requires more precise manufacturing and assembly then a typical box or cantilever (Quickie XTR) frame.[31]

Failures in the Invacare A-6S 1 and A-6S 3 and the Quickie XTR 1 each occurred near a weld, in a heat-affected zone. A heat-affected zone is the region adjacent to a weld in which the material properties of the metal have been altered by the elevated temperatures required to form the weld. When welding high strength aluminum alloys, like those used in wheelchair frame tubing, the

material in the heat-affected zone may become annealed and experience solidification cracking and a reduction of tensile strength.[32] Therefore, the heat-affected zone is usually weaker than the weld and is typically the site of material breakdown. The Invacare A-6S 2 and the Quickie XTR 2 both experienced a fracture along a screw hole in the seat portion of the frame. These were likely caused by concentrated levels of stress that developed around the holes during testing. The failure of the XTR 3 was attributed to a substandard caster mount.

Prior to failure, all A-6S and XTR models passed ISO standards; however, when compared with the performance of previously tested lightweight and ultra lightweight folding-frame wheelchairs, the suspension manual wheelchairs failed to demonstrate significant improvements in fatigue life. Conversely, the ultra lightweight models lasted, on average, approximately 467,175 cycles longer and provided an improved value of about 411 equivalent cycles per dollar. The suspension wheelchairs did demonstrate improved durability compared to the lightweight wheelchairs; however, the difference in equivalent cycles was not significant.

Overall, 66.7% of the suspension wheelchairs were in compliance with the ISO 7176-08 standards, compared to 93.3% of the ultra lightweight wheelchairs and 11.1% of the lightweight wheelchairs. If the Colours Boing results were removed from the analysis, the average number of equivalent cycles completed by the suspension wheelchairs (911,394) would be significantly higher then the lightweight wheelchairs (187,326); however, the number would still fail to match that of the ultra lightweight wheelchairs (1,092,441 cycles).

This contradicts the second hypothesis of this study – that the inclusion of suspension elements would help to extend the lifetime of the wheelchair. One possible explanation, and a concern of suspension wheelchairs, is the additional weight imposed by the suspension system. An increase in weight of several kilograms could elevate the stresses at critical points in the frame and induce premature failure. Another possible explanation for the unexpectedly poor performance of the suspension wheelchairs is that their complex design may increase their susceptibility to failure. Obviously the quick-release caster fork design doomed the performance of the Colours Boing wheelchairs; however, the failures experienced by the Invacare A-6S wheelchairs may also be attributed to a similar conceptual flaw. Though the fractures of the telescoping tubes occurred within the heat-treated regions of the suspension arm weld, they also occurred in the thinnest section of tubing on the frame of the wheelchair. This tubing was likely selected in order to minimize the weight of the additional materials for the suspension; however, it also compromised the integrity of the design. The previously tested Invacare Action XTRA averaged 1,613,013 equivalent cycles while the Invacare A-6S averaged only 597,574 equivalent cycles.

In addition to their unexpectedly low overall durability, the suspension wheelchairs failed to provide a competitive value, based upon our focused testing, to the ultra lightweight wheelchairs. As with the durability results, the suspension wheelchairs demonstrated an improvement in value over the lightweight wheelchairs, but the difference was not significant. Next to durability, the main reason for this is cost. The average cost of the three suspension wheelchairs tested in this study was $2,629, approximately $875 more than the average cost of the four ultra lightweight wheelchairs and $1,684 more than the average cost of the three lightweight wheelchairs used by Cooper and associates.[26,28] The supposed increased durability of the suspension wheelchairs

is one common justification for the increased cost; though as evidenced by this study, the additional expense of a suspension manual wheelchair does not necessarily buy better value.

This study relied on the use of two standardized tests designed to evaluate wheelchair durability. Though these tests have been shown to provide an accurate representation of actual usage,[33] their results should not supercede the knowledge and judgment of clinicians and experienced wheelchair users. Proper wheelchair selection should be based on the capabilities of the individual, the intended use of the wheelchair, and on the best evidence available.[31] Clinicians should also incorporate the mobility preferences of knowledgeable manual wheelchair users, which include those individuals who have successfully integrated the functionality of suspension wheelchairs into their daily mobility activities. However it is also important for clinicians and wheelchair users to understand that suspension manual wheelchairs may not be suitable for everyone. For example, newly injured users require a manual wheelchair that is safe, simple to operate, and can be adjusted to accommodate their advancements in wheelchair skills. Due to their complex designs, suspension manual wheelchairs offer limited adjustability (compared with standard ultra lightweight wheelchairs) and may be inappropriate for the skill level of a novice user. In addition, based on this study, the inclusion of suspension systems may jeopardize wheelchair performance during demanding driving tasks and may require increased maintenance. For experienced users, these findings may not be enough to defer them from selecting a suspension manual wheelchair for everyday use.

Overall, suspension systems may have important implications for reducing the potentially harmful repetitive skeletal loading experienced by manual wheelchair users; however, consumers and clinicians need to be aware that suspension may not increase the reliability of the wheelchair.

Our data and previously published reports indicate that further development of suspension manual wheelchairs is warranted to improve their shock reduction properties and cost effectiveness. In that respect, future studies should be done to evaluate the function of suspension wheelchairs in various conditions (i.e. uneven terrain and during curb descents), and to quantify the response of the suspension elements themselves. In addition, fatigue testing of ultra lightweight rigid wheelchairs should be done to provide a more appropriate basis for evaluating suspension manual wheelchairs. It has been theorized that, due to their construction, folding-frame wheelchairs are capable of absorbing some vibrations; therefore, testing of rigid wheelchairs would establish a baseline from which suspension manual wheelchairs and folding-frame wheelchairs should be measured.

2.4 CONCLUSIONS

This study revealed a lack of significant differences in the overall durability and value between suspension manual wheelchairs and both lightweight and ultra lightweight folding-frame wheelchairs. The inclusion of suspension elements did not significantly improve wheelchair fatigue life; in fact, in some cases, the modifications reduced the total number of equivalent cycles. Significant differences were found amongst the suspension wheelchairs; however this was primarily due to the premature failures of the Colours Boing models. In addition, their increased expense considerably lowered their value in relation to the other types of wheelchairs. Altogether, the study found little evidence to suggest that suspension manual wheelchairs provide advantages in terms of durability or value over non-suspension, folding-frame wheelchairs. Clinicians and users should consider the results of the ANSI/RESNA fatigue

testing before selecting a wheelchair for everyday use. Of course, laboratory test results should be used to augment other available data and clinical experience.

3.0 FUNCTIONAL TESTING OF SUSPENSION AND STANDARD MANUAL WHEELCHAIRS

Beyond demonstrating structural integrity, a wheelchair must adequately satisfy its purpose. For some models that purpose may be to provide high maneuverability or easy transport, for suspension wheelchairs, that purpose is to reduce the transmission of WBV to the rider. Until recently, manual suspension wheelchairs have not been tested for their ability to suppress vibrations. Instead their designs have been considered beneficial for wheelchair users primarily because they feature suspension elements and approaches that have been successful in the bicycle and automobile industries. However, the structural and functional differences between wheelchairs and either bicycles or automobiles suggest the need to adapt common forms of suspension to the specific demands of wheelchairs and their users. Currently no proof of concept or numerical model, which demonstrates the advantages or method of incorporating an adapted system, exists. As a result, the success of wheelchair suspension remains speculative.

Very few studies have been performed to evaluate the capability of manual wheelchair suspension systems. Cooper et al[34] reported that manual wheelchairs with rear suspension systems provided some vibration reduction; however, they tended to transmit peak accelerations in the natural frequency range of humans (4-12 Hz)[35] and were not superior to traditional designs. Results were obtained from a series of tests conducted on an ANSI/RESNA double-drum test machine using a two different test dummies to simulate the wheelchair user. In a

subsequent study of suspension manual wheelchairs, Kwarciak et al[36] suggested that the orientation of the suspension elements rendered the wheelchairs unable to reduce the magnitude of vibrations transmitted to users during curb descents. Peak accelerations obtained from the suspension wheelchairs showed no significant improvement over those obtained from folding-frame wheelchairs. Using force data collected from the same study, Wolf et al[37] showed that absorbed power analysis was unable to identify any differences between the two types of wheelchairs. Force data for this analysis was collected with the SMART^{HUB}, a device that measures the amount of force experienced by the wheelchair at the rear wheel hub.[17] Finally, a study of a European Union-sponsored prototype power wheelchair, in two stages of development, concluded that current suspension systems may not be adequate in suppressing vibration levels responsible for back pain and general discomfort.[38] Frequency analysis revealed the presence of vibrations within the range of human oscillation and resonance frequencies between 3 - 4.5 Hz for both suspension systems.

The purpose of this study was to provide a more thorough functional evaluation of suspension manual wheelchairs. Previous studies have been limited by the small number of wheelchairs included in the evaluation and/or by the methods of data acquisition. The latter limitation concerns the need to test the primary goal of suspension manual wheelchairs – shock vibration suppression. The Sunrise Medical Quickie XTR and the Colours Boing both feature spring-based suspension systems that, as stated earlier, can provide effective shock absorption. Furthermore, suppression of low-level vibrations can be achieved using suspension caster forks[34] and is the recommended focus of specialized wheelchair seating systems.[21,22] Therefore it seems

necessary to examine the performance of wheelchair suspension systems during high-load activities.

Some of the most common high-load activities performed by active wheelchair users are curb descents. Even when curb descents are avoided, vibration loads experienced during regular daily activities can approach magnitudes of 50 m/s^2.[17] The potentially damaging impact of these activities on wheelchairs and their riders has led curb descent testing to be made part of ANSI/RESNA wheelchair fatigue test standards as well as studies of manual and power wheelchairs and their components.[17,19,22,34,36,37,39] For these reasons, curb descents were chosen as an adequate test metric for evaluating the performance of suspension manual wheelchairs. For this study we hypothesized: 1) that mean peak seat accelerations, mean frequency-weighted peak seat accelerations, and impact forces, generated during curb descents, will be significantly lower for suspension manual wheelchairs than for both folding-frame and rigid-frame wheelchairs; 2) while traversing level, uneven terrain, suspension manual wheelchairs will present lower vibration doses at the seat than either folding-frame or rigid-frame wheelchairs; and 3) there will be significant differences in accelerations and forces measured for the three different curb heights (2", 4" and 6") used for testing.

3.1 METHODS

Twelve different manual wheelchairs, four suspension (Everest & Jennings[e] Barracuda, Colours[b] Boing, Invacare[a] A-6S, and Sunrise Medical[c] Quickie XTR), four folding-frame (E&J Epic, Invacare Action Xtra, Kuschall[f] Champion 1000, and Quickie 2), and four rigid-frame (Quickie

GP, TiSport[g] Cross Sport, Invacare A4, and Invacare Top End Terminator), were used to evaluate the effectiveness of wheelchair suspension in reducing shock and vibration transmissibility and impact force. All comparisons were based on vibrations measured at the seat of each wheelchair, and for the curb descents, on the forces measured upon impact with the landing area. For consistency, the same test pilot and seat cushion were used throughout the testing. Each wheelchair was adjusted to meet similar critical dimensions and fitted with identical rear wheels (24" diameter, 65 psi). The horizontal distance between the axle and the backrest was standardized among all wheelchairs. This was done to bring the center of mass (CoM) of the wheelchair and user to a similar position for all systems, and to minimize differences due to the wheelchair set-up (i.e., distance of the rear wheels from the CoM). The distance was specified to be 4 ± 1 cm, based on the range of adjustability of the wheelchairs tested and the similarity to the personal wheelchair of the test pilot. Original equipment manufacturer caster forks were used on every model, as this study sought to identify differences in the base model of each wheelchair. Finally, no adjustments were made to the wheelchair suspensions, since the purpose of adjustment is primarily for rider comfort and not wheelchair performance (within reason). Testing procedures, data collection, and data reduction and analysis for this investigation were composed of two phases.

3.1.1 Phase one: Curb Descents

The first phase of this study compared the transmissibility of shock vibrations and impact forces of the wheelchairs during curb descents of varying heights. The test pilot was asked to descend three different height curbs (2", 4" and 6") with each of the twelve wheelchairs in a randomized order (Figure 9). The curbs were made of a reinforced wooden top (2" thick) and pairs of 2"

thick supports (when needed for additional height). Three sets of trials were performed for each wheelchair, with each set consisting of a randomized order of three different height curb descents (a total of nine descents for each wheelchair) onto a pair of calibrated force plates. The method of descent specified for this testing was based upon the technique used by the test pilot. For each descent, rolling contact with the curb was maintained for as long as possible using a 'wheelie'. The test pilot first balanced the wheelchair on the rear wheels and then descended the curb such that the rear wheels struck the landing area first; thus precluding any confounding data that might otherwise appear if caster impact preceded real-wheel contact. This constrained the definition of a curb descent; however it provided a stable, repeatable method for data collection.

Figure 9. Example of a 4" curb descent.

3.1.1.1 Data collection Acceleration data were collected with an instrumented seat plate, which consists of a 3/8" thick piece of aluminum fitted with a tri-axial accelerometer (Crossbow Technology[h]). During testing, the seat plate was placed on the seat pan of each wheelchair underneath the seat cushion. Data were collected from the accelerometer at 200 Hz. This

provided sufficient sampling of the frequencies (0-50 Hz) of interest for human vibration exposure. During each trial, a person followed the wheelchair in order to support the data logger, which transferred acceleration data to the computer, and to prevent the wires from interfering with testing.

In addition to accelerations, impact forces and wheelchair orientations were measured using a set of calibrated force plates and an Optotrak[i] system, respectively. Two force plates were positioned directly in front of the adjustable curb to comprise the landing area for each descent. Data were recorded continuously from the plates for 5 seconds at 400 Hz using a data-collection program written in LabVIEW[j]. For each trial, the orientation of the wheelchair was determined by tracking the position of six active Optotrak markers, three positioned on the seat portion of frame, one on the axle, and two on the platform surrounding the force plates. A single Optotrak camera was used to record marker positions continuously for 5 seconds at 300 Hz.

3.1.1.2 Data Reduction and Analysis Analysis of acceleration data was limited to vibrations in the vertical direction, normal to the seat of the wheelchair. Subjection to these vibrations presents the greatest risk to the comfort and spinal integrity of seated persons. Consequently, vertical vibrations within the frequency range of human oscillation (4-12 Hz) receive the highest frequency weighting according to ISO 2631-1.[20] Furthermore, suspension manual wheelchairs are designed to suppress vibrations traveling in the vertical direction. A MATLAB[k] script was written to calculate the peak acceleration and frequency-weighted peak acceleration experienced during each curb descent. Application of ISO 2631-1 frequency weighting was consistent with previous analyses of seat acceleration data.[22,33]

Force data were analyzed with a separate program that determined the force recorded from each force plate at impact. These forces were then summed to get a resultant impact force vector. For simplification, any asymmetries in rear wheel contact with the force plate were disregarded. It was assumed that the proximity of the both impacts would not be great enough to be perceived by the test pilot; and that the forces generated from each descent would present as a single shock vibration. Incidentally, the test pilot was instructed to descend each curb symmetrically.

Optotrak data were used to calculate the wheelchair frame angle, and for suspension wheelchairs, the suspension angle, at impact with the force plates. The two frame markers positioned farthest from the backrest were used to construct a line representing the plane of the seat. The third marker was disregarded due to instances of marker fallout in several trials. A similar procedure was used to construct a line representing the surface of the force plate using the two platform

markers. Frame angle was calculated using the dot product of the 'seat line' and the 'plate line' and their respective magnitudes.

The suspension angle refers to the angle at which the axle approaches the seat during loading. For three of the four suspension wheelchairs, this angle of approach was determined by measuring the angle of the suspension elements, with respect to the ground, while the wheelchair was in its standard orientation (all four wheels on the ground). For the Invacare A-6S, which features a ratcheting suspension mechanism (Figure 1), the approach angle was found by measuring the movement of a point on the seat as the wheelchair was loaded. By summing the resting suspension angle with the angle of the frame at impact, the angle of the suspension at impact was determined. The suspension angle at impact was then compared to the angle of the impact force vector as a means to explain the acceleration and force data and to evaluate the appropriateness of the suspension systems.

3.1.2 Phase two: Level Uneven Surface Testing

To provide a baseline for comparing all wheelchairs tested in this study, subsequent testing was performed on a level, uneven surface. The surface was composed of three blind guidance tiles (3' x 4' each), typically used to help visually impaired persons identify ledges and other important ground surfaces. Each tile consists of offset rows of truncated half-domes that, when traversed in a wheelchair, provide a consistent source of vibration. For each trial the test pilot was asked to traverse the strip of tiles at 1 ± 0.2 m/s (Figure 10). Speed was checked with a stopwatch and any trial failing to meet the speed restrictions was redone. Three successful trials were obtained for each of the twelve wheelchairs, tested in a randomized order.

3.1.2.1 Data collection Consistent with phase one, acceleration data were collected at the seat of each wheelchair with an instrumented seat plate at a rate of 200 Hz. In addition, an Optotrak system was used to track the position of four active Optotrak markers, three positioned on the seat portion of frame and one on the axle. Marker positions were recorded continuously for 4 seconds at 300 Hz.

Figure 10. Example of blind guidance tile testing.

3.1.2.2 Data Reduction and Analysis Vertical acceleration data obtained from the instrumented seat plate were used to calculate the vibration dose value (VDV):

$$VDV = \left[\int a_w^4(t)dt\right]^{\frac{1}{4}}$$

where a_w refers to the frequency-weighted vertical acceleration. Traditionally, a_w represents the resultant acceleration that is created from tri-axial acceleration data.[22,34] However, this study focused on the ability of suspension manual wheelchairs to suppress vertical vibrations;

therefore, data analysis included only frequency-weighted vertical accelerations, which were found using the same ISO 2631-1 frequency-weighting algorithms used in previous studies of wheelchair vibration.[22,34] The continuous-time integral presented in the VDV equation was approximated with trapezoidal numerical integration.

The VDV was selected for this analysis because it provides a reliable cumulative measure of vibration and has been found to correlate well with some responses to vibration.[1] Although results published by Lundström et al[40] suggest that absorbed power provides a more appropriate measure of vibration exposure, because it considers the dynamic forces applied to the body, VDV is regarded throughout the literature as a dependable method for vibration analysis.[7,22] Furthermore, considering the source of vibration and the methods of data collection employed by this study, VDV presented the most appropriate metric for analysis.

Optotrak data for this phase were used to examine the VDV calculated for each wheelchair. The two markers farthest from the backrest were used to construct a line representing the seat plane. For this phase no ground markers were used, as the guidance tiles were taped directly to the concrete floor (which coincides with the x-y plane of the Optotrak system). A horizontal unit vector was created in MATLAB to represent the plane of the ground. Frame angle was calculated using the dot product of the seat line and the ground line and their respective magnitudes. Suspension angle was not calculated for uneven surface testing.

3.1.3 Statistical Analysis

Mixed model analysis was used to compare the results obtained in both phases and test the hypotheses that suspension manual wheelchairs transmit lower levels of vibration and force than standard folding- and rigid-frame wheelchairs. For each mixed model, the fixed and random factors were represented by wheelchair type (suspension, folding, or rigid) and curb height, respectively. Differences in least square means, with a Bonferroni adjustment, were used to identify individual differences between the wheelchairs. All models were subsequently rerun with wheelchair weight included as an additional random factor. This was an experimental point of analysis used to determine how weight influenced the results. Finally, mixed models were run with curb height set as the fixed factor and wheelchair type set as the random factor to determine the significance of the three different curb heights. All analyses were performed using SAS with a level of significance set at 0.05.

3.2 RESULTS

3.2.1 Curb descent testing

For clarification, all assessments of acceleration data are based on magnitude and not sign. The mean peak accelerations and mean frequency-weighted peak accelerations calculated for each wheelchair for each curb height are presented in Table 3. Reliable interclass correlation coefficients for the data could not be obtained because of the small number of individual wheelchair trials (3) for each curb height and the inconsistencies in performance within each wheelchair type. Based on mixed-model analysis, significant differences were found between suspension wheelchairs and both folding- and rigid-frame wheelchairs in mean peak acceleration

(p = 0.0243; p = 0.0253) and mean frequency-weighted peak acceleration (p < .0001; p = 0.0045). As a group, suspension wheelchairs presented the lowest mean peak accelerations for each curb descent; however, individually they did not represent the four best wheelchairs, referring to those wheelchairs that transmitted the smallest amount of vibrations to the seat. For each curb descent at least one standard wheelchair, most frequently the rigid-frame Invacare Top End Terminator, posted lower accelerations then one or more of the suspension wheelchairs. In addition, the reduced accelerations measured for the suspension wheelchairs became less apparent as the height of the curb descent increased (Figure 11).

Table 3: Mean Peak and Mean Frequency-Weighted Peak Accelerations

		Mean Peak Accelerations			Mean Freq-Weighted Peak Accelerations		
Type/Model		2"	4"	6"	2"	4"	6"
Suspension	A6S	-19.50 ± 2.42	-41.26 ± 8.16	-68.45 ± 16.77	-8.45 ± 2.14	-16.95 ± 1.69	-23.77 ± 3.95
	BAR	-27.50 ± 1.92	-33.26 ± 7.62	-61.41 ± 15.98	-12.16 ± 0.88	-17.25 ± 4.06	-28.94 ± 7.97
	BNG	-19.50 ± 0.55	-31.66 ± 5.29	-51.18 ± 11.73	-8.87 ± 0.58	-16.47 ± 2.21	-21.28 ± 3.13
	XTR	-16.62 ± 0.55	-27.82 ± 4.54	-32.62 ± 4.54	-5.03 ± 1.18	-10.61 ± 1.57	-14.75 ± 1.16
Folding	EPC	-28.46 ± 5.84	-51.82 ± 12.15	-56.61 ± 7.20	-13.08 ± 4.61	-26.65 ± 5.29	-31.46 ± 6.22
	IAX	-31.66 ± 3.63	-47.98 ± 9.47	-54.38 ± 11.68	-15.36 ± 1.43	-26.53 ± 4.95	-29.26 ± 3.67
	KUS	-35.18 ± 6.92	-46.38 ± 5.46	-69.41 ± 6.94	-17.79 ± 2.58	-23.29 ± 3.34	-35.53 ± 3.57
	QU2	-30.70 ± 9.07	-39.98 ± 8.20	-45.42 ± 4.33	-14.17 ± 3.84	-20.06 ± 4.25	-24.67 ± 5.46
Rigid	IA4	-33.58 ± 12.23	-46.70 ± 11.52	-59.49 ± 13.62	-14.84 ± 3.91	-20.15 ± 4.89	-33.46 ± 3.69
	QGP	-31.02 ± 5.79	-47.02 ± 2.00	-61.73 ± 18.82	-12.89 ± 4.26	-23.08 ± 4.82	-29.74 ± 7.33
	TIS	-31.34 ± 2.93	-41.90 ± 8.71	-52.14 ± 26.13	-14.72 ± 1.21	-22.43 ± 2.78	-20.01 ± 7.40
	TER	-24.94 ± 3.46	-32.94 ± 5.34	-74.53 ± 10.26	-11.99 ± 0.77	-13.61 ± 5.73	-33.98 ± 2.20

The differences in mean peak acceleration between the suspension wheelchairs and the folding- and rigid-frame wheelchairs, for 6" curb descents, were 3.04 m/s and 8.56 m/s, respectively. These were the smallest differences between the wheelchair types for any of the three curb heights. On the other hand, the differences in the frequency-weighted accelerations between the

different wheelchair types increased between 2” and 6” curb descents, mostly due the superior performance of the Quickie XTR, which had the lowest frequency-weighted accelerations for all three curbs. This is a critical point in terms of wheelchair performance. Considering that the ISO 2631-1 frequency-weighting system emphasizes perturbation frequencies to which the human body is most sensitive, analysis of frequency-weighted accelerations provides a good indication of the injury risk associated with each wheelchair for each curb descent.

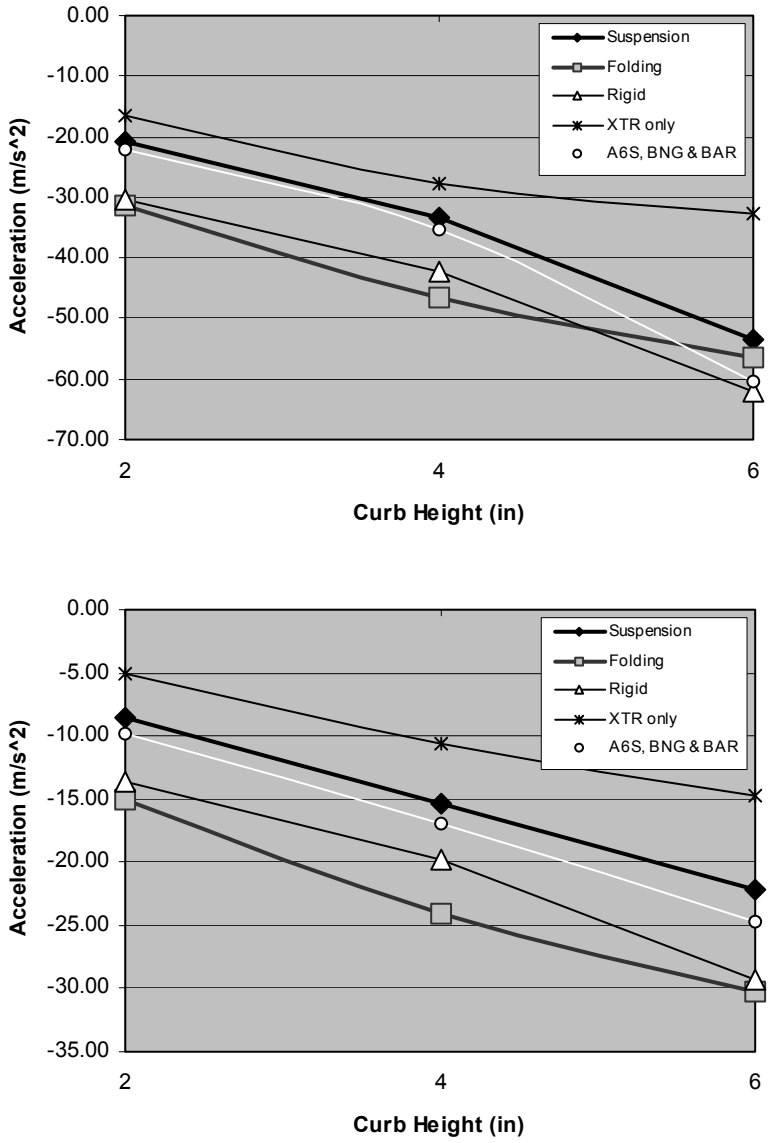

Figure 11. Mean peak accelerations (top) and frequency-weighted peak accelerations (bottom) averaged for each wheelchair for each curb height.

The peak vertical forces, averaged for each wheelchair for each curb height, are shown in Figure 12. As with the acceleration data, interclass correlation coefficients could not be determined for the force data. Based on mixed model analysis, wheelchair type was not a significant factor ($p = 0.352$) in distinguishing the forces measured for each wheelchair; however, significant differences were found between individual wheelchairs (Table 4). Typically, significant differences in peak force were found in comparisons against folding-frame wheelchairs. The forces measured from the Quickie XTR were significantly lower than the forces measured from all four folding-frame wheelchairs. With respect to the rigid-frame wheelchairs, only the XTR and the TiSport Cross Sport (rigid) demonstrated significantly lower mean peak force(s).

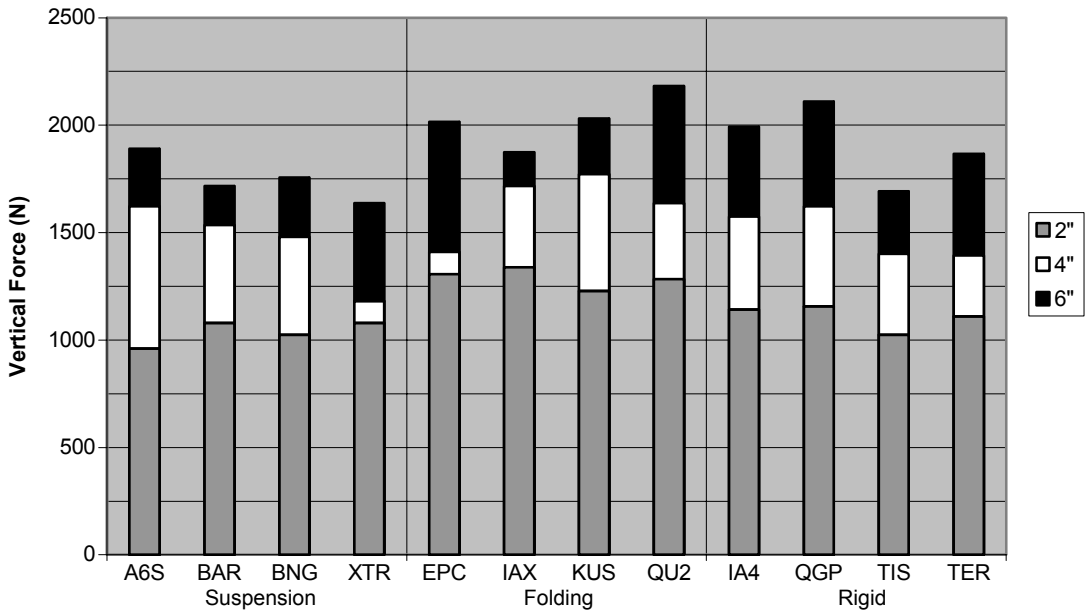

Figure 12. Mean peak vertical force measurements for each wheelchair for each curb height.

Table 4: Significant Differences Between Wheelchairs With Respect to Mean Peak Force

Wheelchair 1	Wheelchair 2	Adjusted p
Colours Boing	Kuschall Champ 1000	0.0496
	Quickie 2	0.0057
Quickie XTR	E&J Epic	0.0066
	Invacare Action Xtra	0.0002
	Kuschall Champ 1000	<.0001
	Quickie 2	<.0001
	Invacare A4	0.0099
	Quickie GP	0.0003
Top End Terminator	Quickie 2	0.0376
TiSport Cross Sport	Invacare Action Xtra	0.0099
	Kuschall Champ 1000	0.0048
	Quickie 2	0.0004
	Quickie GP	0.0195

Note: Wheelchair 1 represents the wheelchair for which the lower mean peak force was measured.

The mean peak forces shown in Figure 12 were calculated from data recorded from both force plates throughout each curb descent. Examples of truncated force data collected from each type of wheelchair for each curb height are presented in Figures 13-15. Each of these data sets was reduced to show the component forces leading up to (0.25 second prior) and following (0.50 second after) the maximum measured force associated with impact. Both symmetric and asymmetric impacts are evident in the force data trials, exemplifying the imperfections and inconsistencies in the curb descents performed by the test pilot.

Through visual inspection of the data (Figures 13-15), it was apparent that the peak force experienced by the wheelchair and rider was typically preceded by a spike or plateau, caused by deformation (energy absorption) of the wheelchair and suspension system (where applicable) on impact. The amount of energy absorbed was reflected in the severity of the change in force and was dependent on the characteristics of the wheelchair. Based on their design, suspension wheelchairs exhibited the largest drop in force, especially for 4” and 6” curb descents. Both folding- and rigid-frame wheelchairs provided some energy absorption; however, they saturate

much more quickly and often present only a slight reduction in force. From the plots in Figures 13-15 it appears that saturation for standard, non-suspension wheelchairs occurred soon after the first wheel impacted the force plate. Incidentally the use of pneumatic rear tires provided some energy absorption for all trials.

For the purposes of this study, only the maximum force was used to compare wheelchair performance, primarily because larger forces present a greater threat to the health and comfort of wheelchair users. The initial impact, represented by the initial drop in force data, may be used to characterize the function of the wheelchair at impact; however, it was not a reliable predictor of performance or maximum force. It is suspected that inconsistencies between the descents, particularly in the position of the center of mass of the wheelchair/test pilot, the symmetry of the rear wheels, and the orientation of the wheelchair at impact, greatly affected the time and magnitude of the initial impacts. On the other hand, maximum force appeared to be affected mainly by curb height, the weight of the wheelchair and test pilot, and the capabilities of the wheelchair. Therefore initial impacts were disregarded in this analysis.

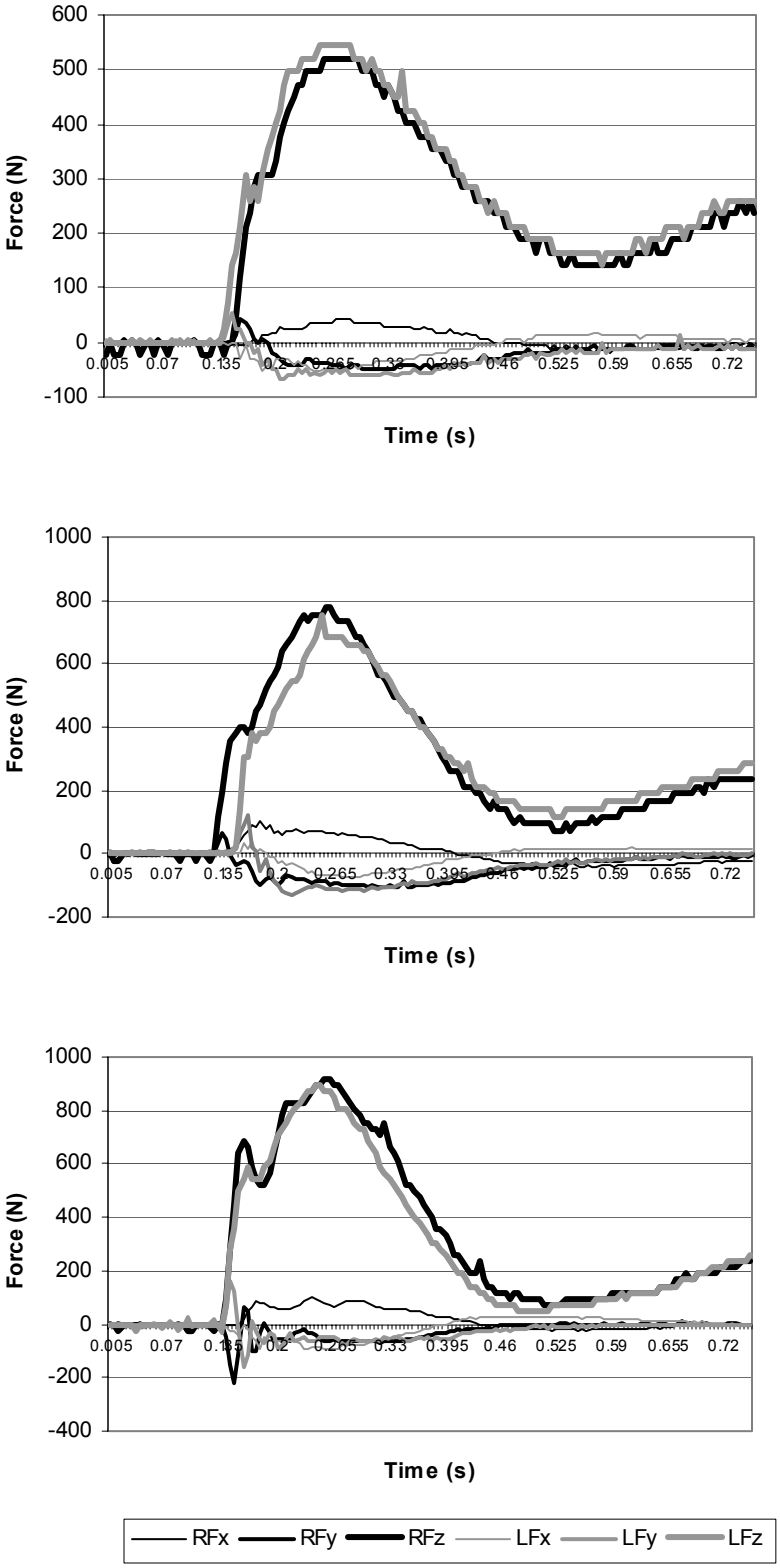

Figure 13. Examples of force data collected from the E&J Barracuda (**suspension**) during 2" (top), 4" (middle), and 6" (bottom) curb descents; where RFx, RFy and RFz represent the component forces measured from the right force plate and LFx, LFy and LFz represent the component forces measured from the left force plate.

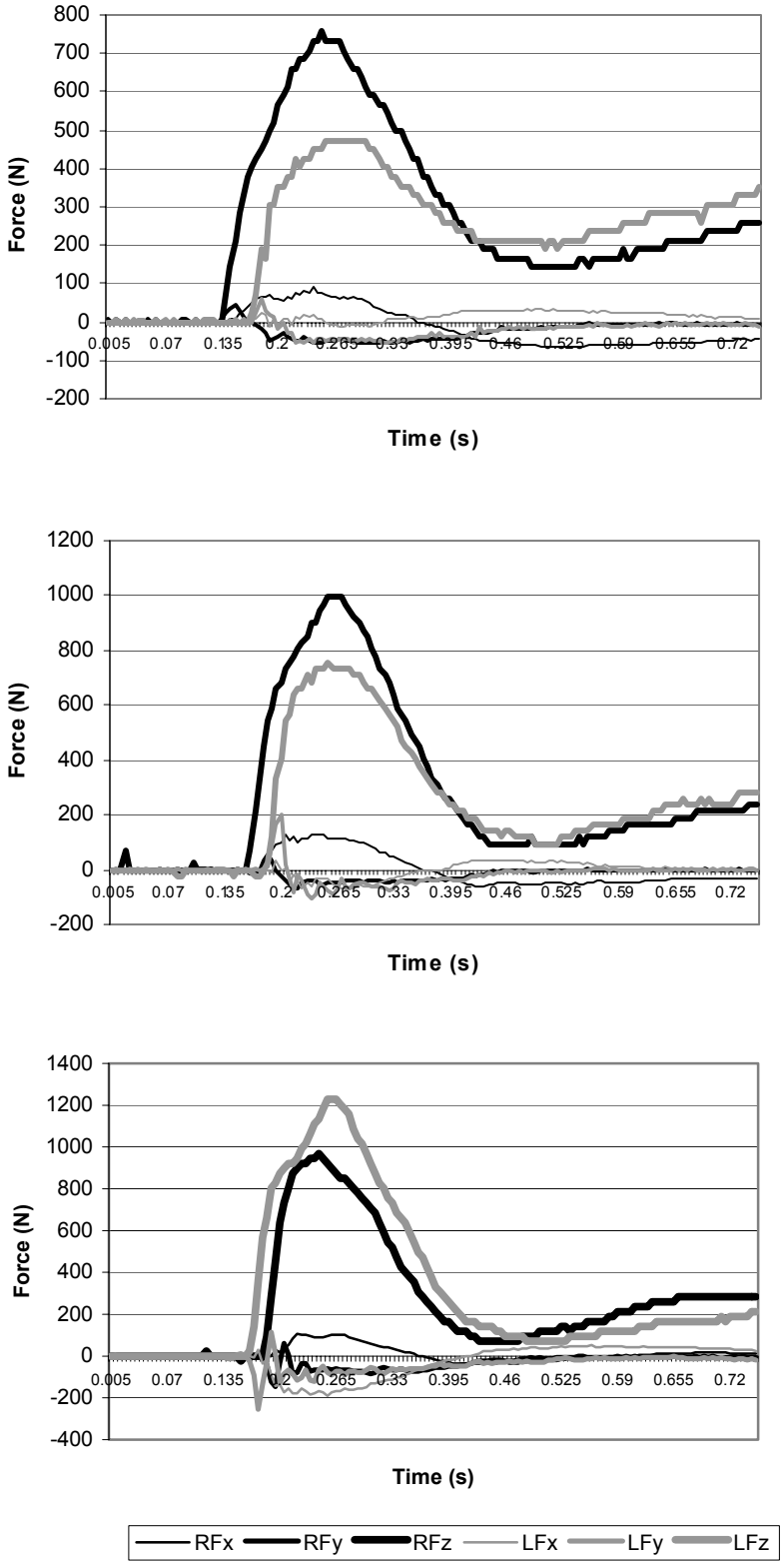

Figure 14. Examples of force data collected from the Kuschall Champion 1000 (**folding**) during 2" (top), 4" (middle), and 6" (bottom) curb descents; where RFx, RFy and RFz represent component forces measured from the right force plate and LFx, LFy and LFz represent components measured from the left force plate.

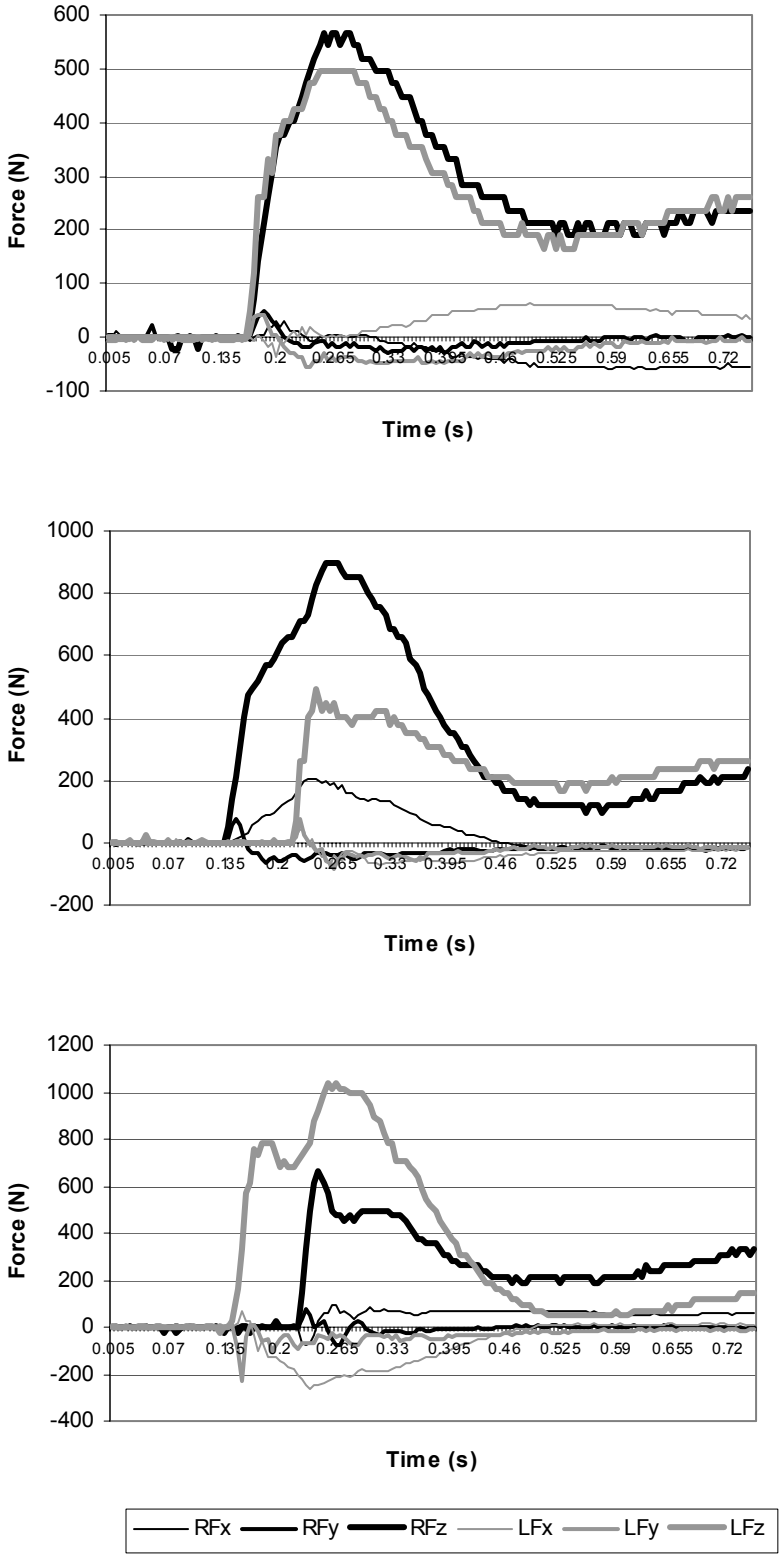

Figure 15. Examples of force data collected from the TiSport Cross Sport (**rigid**) during 2" (top), 4" (middle), and 6" (bottom) curb descents; where RFx, RFy and RFz represent the component forces measured from the right force plate and LFx, LFy and LFz represent the component forces measured from the left force plate.

3.2.2 Blind Guidance Tile Testing

The mean VDV calculations, performed with the acceleration data obtained from blind guidance tile testing, is presented in Table 5. Mixed model analysis of the dose values found significance

Table 5: Mean VDV for Each Wheelchair and Wheelchair Type

Type	Model	Mean VDV	Type Avg VDV
Suspension	A6S	15.11 ± 0.50	19.67 ± 6.62
	BAR	17.88 ± 2.43	
	BNG	15.73 ± 0.71	
	XTR	29.97 ± 3.94	
Folding	EPC	18.21 ± 0.95	16.01 ± 1.74
	IAX	13.97 ± 0.16	
	KUS	16.20 ± 1.05	
	QU2	15.67 ± 0.90	
Rigid	IA4	17.16 ± 0.96	17.49 ± 1.37
	QGP	19.14 ± 1.15	
	TER	17.21 ± 1.01	
	TIS	16.46 ± 1.09	

between wheelchair types, due to the highly significant differences ($p < .0001$) between the Quickie XTR and all other wheelchairs. The particularly high value of VDV calculated for the XTR was nearly 57% higher than the largest VDV amongst the remaining wheelchairs (Quickie GP – 19.14 m/s^2). As a result, the suspension wheelchairs had the worst average VDV of all three types. Without including the XTR, the suspension wheelchairs would have a VDV of about 16.24 m/s^2. In contrast, the average VDV for the folding-frame wheelchairs was greatly helped by the inclusion of the Invacare Action Xtra, which had the lowest overall VDV (13.97 m/s^2). Incidentally, the Action Xtra was the only wheelchair other than the XTR to show significance; it had a significantly lower VDV ($p = 0.0318$) than the Quickie GP. Without these two extreme cases, the overall average VDV was 16.88 m/s^2 with a standard deviation of 1.27.

3.2.3 Differences in Curb Height

The inclusion of curb height in the mixed model analysis allowed comparisons to be drawn between the curbs based on the collected data. From these models, significant differences were found between the three curb heights ($p \leq 0.006$) in both acceleration and force data. This justifies the use of the three different curbs as unique perturbation tests and validates the investigation.

To quantify the effects of curb height on the acceleration and force data obtained from the curb descents, multiple regression analyses were performed using SAS. Wheelchair weight was included as a second variable to determine the strength of curb height as a predictor of each criterion. For mean peak acceleration, the regression model ($F = 58.37$; $R^2 = 0.5265$; $p < .0001$) indicated that curb height was a reliable predictor ($p < .0001$); however, weight was found to be uncorrelated ($p = 0.895$). For the mean peak vertical force, the regression model ($F = 170.22$; $R^2 = 0.766$; $p < .0001$) indicated that both curb height ($p < .0001$) and weight ($p = 0.0016$) were reliable predictors. From these analyses, it is apparent that curb height strongly influenced the data obtained during curb descent testing.

3.3 DISCUSSION

3.3.1 Curb Descents: Mean Peak Accelerations and Mean Peak Forces

Each of the four suspension manual wheelchairs tested in this study presents a unique approach to vibration reduction; however, all of the models seem focused on reducing vertical vibrations, particularly shock vibrations, acting normal to the seat of the wheelchair. Based on the expected

ability and experience level of a suspension manual wheelchair user, curb descents were selected as a means by which comparisons of shock vibration transmissibility and impact force could be made. Curb descents demand stability and control, often requiring the user to perform and maintain a wheelie in order to avoid falling forward out of the wheelchair on impact with the lower surface. During this process, the benefit of the suspension system may be compromised due to the orientation of the wheelchair.[36] For this reason, Optotrak markers were used to identify the position of the wheelchair with respect to the test surface. This provided an approximation of wheelchair frame angle that was used to help quantify the results.

Examples of frame angle (with axle height) for each of the three curb descents, calculated using data collected from the Quickie XTR, are shown in Figure 16. For easier visual inspection, the data were truncated to show frame angle and axle height leading up to, and just following rear wheel impact. In this analysis, rear wheel impact was defined as the point where the axle height reached its initial minimum value. Complete sets of axle marker data show an additional decrease in axle position following the initial minimum. This lower axle height was attributed to tire compression and was disregarded in this analysis. Using the point at which the initial minimum was reached, the corresponding frame angle at impact was determined.

Prior to impact, variability in frame angle was apparent in many trials, particularly in the top plot (2" curb descent) of Figure 16. It was determined that these changes in angle were not related to curb height, but instead to the conditions preceding the trial. Since the test pilot had to perform a wheelie before descending the curb, any hesitation in performing the descent resulted in some instability, noted by the fluctuation in frame angle. One important point to consider is the

change in angle that occurs during descent and impact. As the wheelchair descends, frame angle increases, suggesting the test pilot allowed the wheelchair to roll underneath the CoM of the system for added stability. In the plots of the 4" and 6" curb descents, a drop in frame angle occurs after the maximum value is reached. This drop is attributed to the downward rotation of the front of the wheelchair as it pivoted about the rear wheels during the descent. Evidence of this rotation was more prominent in the higher curbs because they provided additional potential energy to the system.

The drop in frame angle observed for the higher curb descents was accompanied by a small increase in axle height, which occurred immediately before the axle reached its initial minimum height. It is presumed that the increase in axle position was caused by contact with the force plate and subsequent energy absorption by the system, which would relieve some of the force placed on the wheels. Based on this presumption, it can be argued that the peak of this increase in axle height should represent the impact and not the initial minimum value. However, due to the small time delay between the peak and the initial minimum value, and the difficulty in identifying the peak in the data collected from the non-suspension wheelchairs, the minimal value was used to represent rear wheel impact.

Fro this analysis, the most important point of the angle data to consider was the value of the seat angle at impact (Table 6). For each suspension manual wheelchair, this value was used to determine the corresponding angle of the suspension system at impact. It also indicates the angle of the wheelie performed for each curb height.

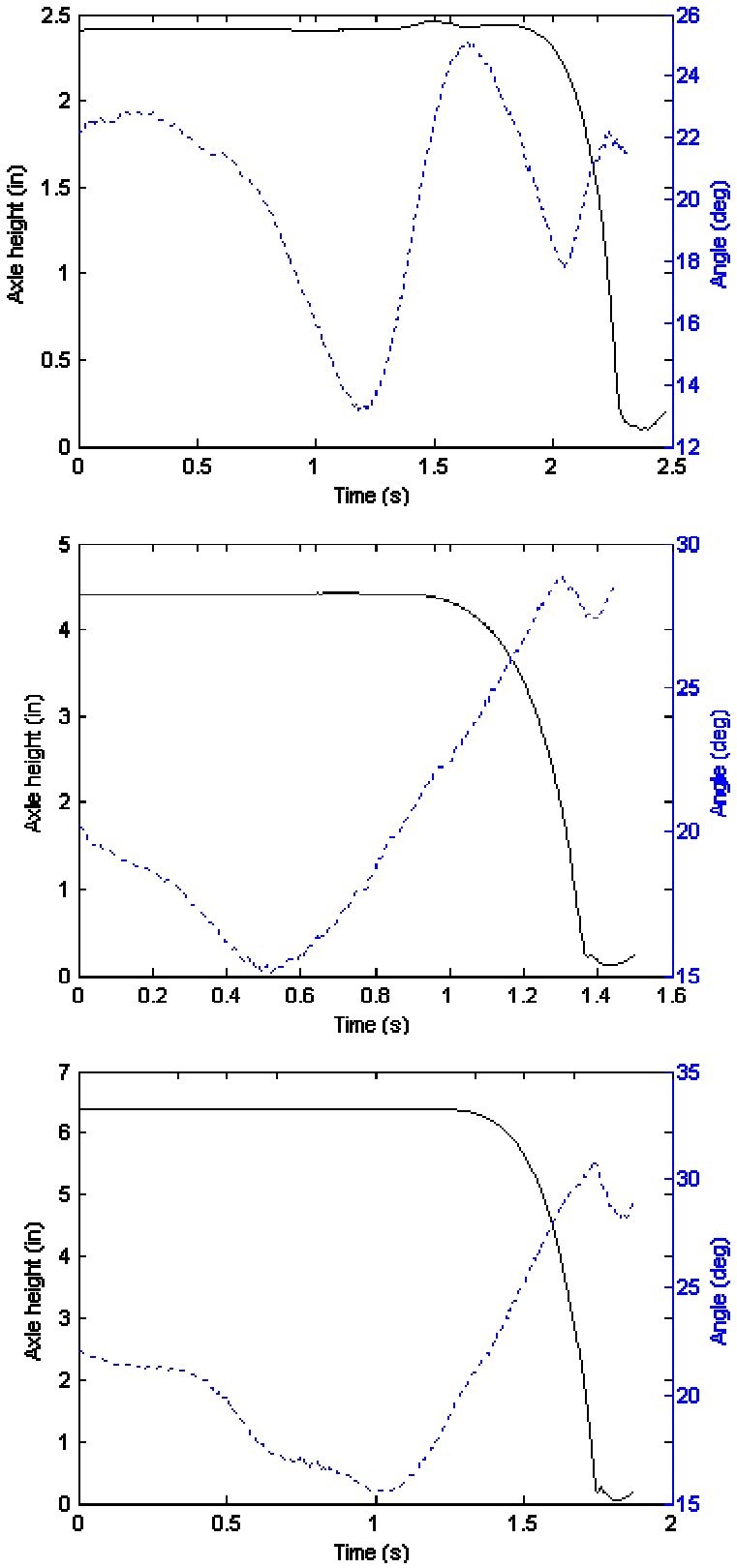

Figure 16. Examples of Quickie XTR frame angle (---) and axle height (—) for 2" (top), 4" (middle), and 6" (bottom) descents.

Table 6: Mean Frame Angles for Each Wheelchair at Impact

	Mean Impact Angle		
Model	2”	4”	6”
A6S	27.64	31.93	34.39
BAR	28.51	35.55	32.87
BNG	24.76	30.23	33.12
XTR	26.70	27.72	27.83
EPC	22.82	23.07	26.87
IAX	20.97	24.29	26.06
KUS	22.18	25.34	26.92
QU2	23.24	28.29	27.97
IA4	14.29	18.64	19.77
QGP	18.14	21.53	23.95
TER	24.10	32.43	28.93
TIS	23.24	30.55	31.29
Average	23.05 ± 4.21	27.23 ± 5.18	28.19 ± 4.31

Note: The average angles and their standard deviations was derived from all 106 values (2 were unusable)

By summing the frame angle at impact with the resting suspension angle, the suspension angle at impact was found. Table 7 shows the mean suspension angle at impact for each suspension wheelchair for each curb height as well as the differences between the suspension angle at impact and the resting suspension angle for each curb height. Based on the similarities in the latter set of values, especially for the 2” curb descents, it appears that the different curb heights similarly affected the orientation of each wheelchair.

Table 7: Nominal Suspension Angles and Mean Angles of Suspension at Impact

Model	Suspension Angle	Mean Suspension Angle at Impact			Difference Between Suspension Angle at Impact and Resting Suspension Angle		
		2”	4”	6”	2”	4”	6”
Quickie XTR	82.0	108.7 ± 2.73	109.7 ± 2.55	109.8 ± 0.82	26.7 ± 2.73	27.7 ± 2.55	27.8 ± 0.82
Invacare A-6S	85.2	112.8 ± 0.26	117.1 ± 2.14	119.6 ± 3.99	27.6 ± 0.26	31.9 ± 2.14	34.4 ± 3.99
Colours Boing	101.0	125.8 ± 2.26	131.2 ± 1.18	134.1 ± 3.65	24.8 ± 2.26	30.2 ± 1.18	33.1 ± 3.65
E&J Barracuda	101.5	130.0 ± 4.46	137.1 ± 0.50	134.4 ± 0.73	28.5 ± 4.46	35.6 ± 0.50	32.9 ± 0.73

Assuming that the vibration-reducing capability of each suspension system is maximized for accelerations traveling along the suspension angle, then each of the mean suspension angles

listed in Table 7 indicates the ideal impact (force) angle for the system. In this study, the impact force was taken to be the vertical force component of the impacts measured by the force plates (See 3.3.2 Justification For Exclusive Use of Vertical Force).

The relative proximity of the XTR suspension to 90º at impact may explain why it was the best overall wheelchair in terms of mean peak acceleration transmission and peak vertical force for all curb descents. The E&J Barracuda and the Colours Boing, the wheelchairs with the two highest suspension angles at impact, produced average overall mean peak accelerations and moderately below-average forces. For these wheelchairs, the suspension angle fit the data; however, the angle of the Invacare A-6S, second lowest among suspension wheelchairs, did not translate into predictable results. For 6" curb descents, the A-6S produced the third highest mean peak acceleration of all wheelchairs tested. This suggests that the performance of suspension wheelchairs during curb descents was also dependent on the type of suspension elements used.

Two of the four suspension wheelchairs, the A-6S and the Barracuda, feature elastomer-based systems. Both wheelchairs include multiple elastomers to provide independent suspension. The Colours Boing also features independent suspension, using two metal springs to regulate compression of its multi-linkage frame. And finally, the Quickie XTR utilizes a single RockShox® mountain bike shock to couple the axle and lower frame to the seat. This represents the most sophisticated suspension element used by the four wheelchairs. Based on the data collected from the first phase of this study, each system has advantages and limitations.

The data collected from 2" curb descents tended to corroborate the original notion that wheelchair performance was determined by suspension angle at impact. The two wheelchairs with the lowest impact angles, the XTR and the A-6S, had the lowest mean peak accelerations and mean frequency-weighted peak accelerations, followed closely by the Boing and finally the Barracuda. As a side note, the Barracuda demonstrated the worst performance of all suspension wheelchairs. It is suspected that the extreme posterior position of the suspension (Figure 17), most rearward of any wheelchair, did not allow for much energy absorption; in fact, the Barracuda transmitted more harmful vibrations (within 4-12 Hz range) than the rigid-frame Invacare Top End Terminator. Also the Barracuda is the only wheelchair with a solid seat pan, which most likely resulted in higher vibration transmission.

Figure 17. Elastomer suspension system of the E&J Barracuda.

Overall the performances of the suspension wheelchairs based on acceleration data were mimicked by the force data, with the exception for the XTR, which had the highest vertical force of the group. Considering the low mean accelerations experienced for the same curb height, the

vertical force measurements for the XTR suggests that the shock absorber is reasonably well positioned to reduce vibrations from small curb descents. More importantly, the shock absorber was the most adequate suspension element for reducing the magnitude of vibrations in the frequencies of human oscillation.

On 4" curb descents, the limitations of the suspension manual wheelchairs became apparent. Due to large increases in measured acceleration and force, the A-6S became the worst suspension wheelchair in terms of both mean peak acceleration and mean peak vertical force. Interestingly, it remained one of the best wheelchairs in terms of mean frequency-weighted peak acceleration, exemplifying the ability of the elastomers to reduce and/or properly shift low-frequency vibration. Meanwhile the Boing and the Barracuda demonstrated reduced vibrations, but failed to outperform the Terminator, which presented lower mean peak acceleration than the Barracuda and lower mean frequency-weighted accelerations than both wheelchairs.

Considering these results, it is important to note that frequency-weighted accelerations become more relevant in the assessment of wheelchair suspension as curb height increases. The impacts associated with higher curb descents (4" and 6") excite the wheelchair with more frequency modes, which are presumably beyond the natural frequency range of the human body. So, while peak acceleration may increase dramatically between 2" and 6" curb descents, the frequency-weighted accelerations may not experience proportional increases. In other words, manual wheelchair users may not be as sensitive or vulnerable to the additional, higher frequency modes generated from 4" and 6" curb descents. Therefore, it is important to concentrate more on frequency-weighted accelerations, which isolate those vibrations that pose the greatest risks of

pain and secondary injury. Despite this focused attention, attempts should be made to reduce the transmission of all vibrations frequencies.

In terms of the forces generated from 4" curb descents, all three suspension wheelchairs (excluding the XTR) presented higher mean peak vertical forces than the folding-frame E&J Epic and the rigid-frame Terminator and TiSport Cross Sport. At this curb height, the lighter weight of the rigid-frame wheelchairs and the flexibility of the folding-frame Epic became a more dominant factor then the presence of most suspension systems. Furthermore, it appears that the increase in frame angle, required for safe descent of the larger curb height, limited the capability of the suspension systems. This seems to hold true for all suspension wheelchairs except the XTR, which presented the lowest mean acceleration and mean peak vertical force for all wheelchairs.

Results of the 6" curb descents help to further establish and explain the trends in the capability of wheelchair suspension. In terms of mean peak vertical force, the suspension wheelchairs provided improved reduction over both folding- and rigid-frame wheelchairs. However, in terms of mean peak accelerations, the suspension wheelchairs performed more closely then ever to the standard wheelchairs. The unexpectedly high values measured for the A-6S and the Barracuda, greatly increased the mean peak acceleration average for the group. As expected, the 6" curb height yielded the highest overall mean suspension angle at impact (~124.5°). At this angle, the elastomer-based suspensions were relatively ineffective at reducing accelerations, although they did provide reduction in frequency-weighted accelerations. Surprisingly, the Barracuda had the third lowest mean peak vertical force (the A-6S was seventh), suggesting that while the

elastomers were capable of some vibration reduction, they tended to transmit most of the resulting vibrations to the seat. Further analysis is required to determine how location and orientation affect the ability of elastomers to reduce accelerations and force associated with curb descent. In general, though the results indicate that elastomer suspension systems are not useful for suppressing random high-load shock vibrations, they should be considered for their ability to reduce force and suppress low-frequency oscillations. Perhaps elastomers could be used to couple sections of the wheelchairs where vibration reduction is crucial (i.e. the seat and the backrest).

Contrary to the A-6S and the Barracuda, the remaining two suspension manual wheelchairs were relatively successful in reducing acceleration and vertical force for 6" curb descents. The success of the XTR is attributed to a low suspension angle and the most capable suspension element of the four tested in this study. The XTR also had the smallest suspension angle at impact on every curb descent as well as the smallest change in angle from 2" to 6" curb descents (1.13°). The small angles were possible, due to the position of the CoM, which was the farthest back of any suspension wheelchair. On the other hand, the success of the Boing is suspected to be due to the long springs used in the suspension. During 4" and 6" curb descents, lateral bending of the spring may have provided some of the reduction in acceleration and force. Another possible explanation for the improved performance is the fact that the springs don't include dampers, allowing for unimpeded travel. Therefore, despite their high angle at impact, the springs may have still have experienced considerable compression and thus provided some energy absorption.

As an additional observation, on 6" curb descents, folding-frame wheelchairs had a lower overall mean peak acceleration (-56.45 m/s^2) then the much lighter rigid-frame wheelchairs (-61.97 m/s^2). This corroborates the hypothesis that, due to their collapsible frame, folding-frame wheelchairs are capable of vibration reduction. Even on 4" curb descents the Quickie GP had a lower mean peak acceleration then four other wheelchairs (three rigid, one suspension). This capability did not translate into a reduction of frequency-weighted accelerations.

Further testing of the suspension manual wheelchairs is required to fully understand their benefits. Each suspension system demonstrated some benefit(s) over standard, non-suspension wheelchairs; however, the systems were not optimal. The significant differences found between the wheelchair types were mostly due to the supremacy of the XTR. The other three suspension manual wheelchairs presented very few improvements over folding- and rigid-frame wheelchairs, especially from higher curb heights. And though it can be argued that curb descents present a more extreme obstacle for wheelchair users, in terms of both wheelchair orientation and impact force, it is presumed that a properly adapted suspension manual wheelchair should be able to adequately suppress the energy generated from impact with the landing surface. Future development of wheelchair suspension must address the impact of curb descents and other particularly demanding obstacles.

3.3.2 Justification For Exclusive Use of Vertical Force

The isolation of vertical force was based on observed trends in force plate data. Plots of the x, y, and z components of force are shown in Figure 18. It was expected that different curb heights would correspond to different impact forces, particularly with respect to magnitude. However no

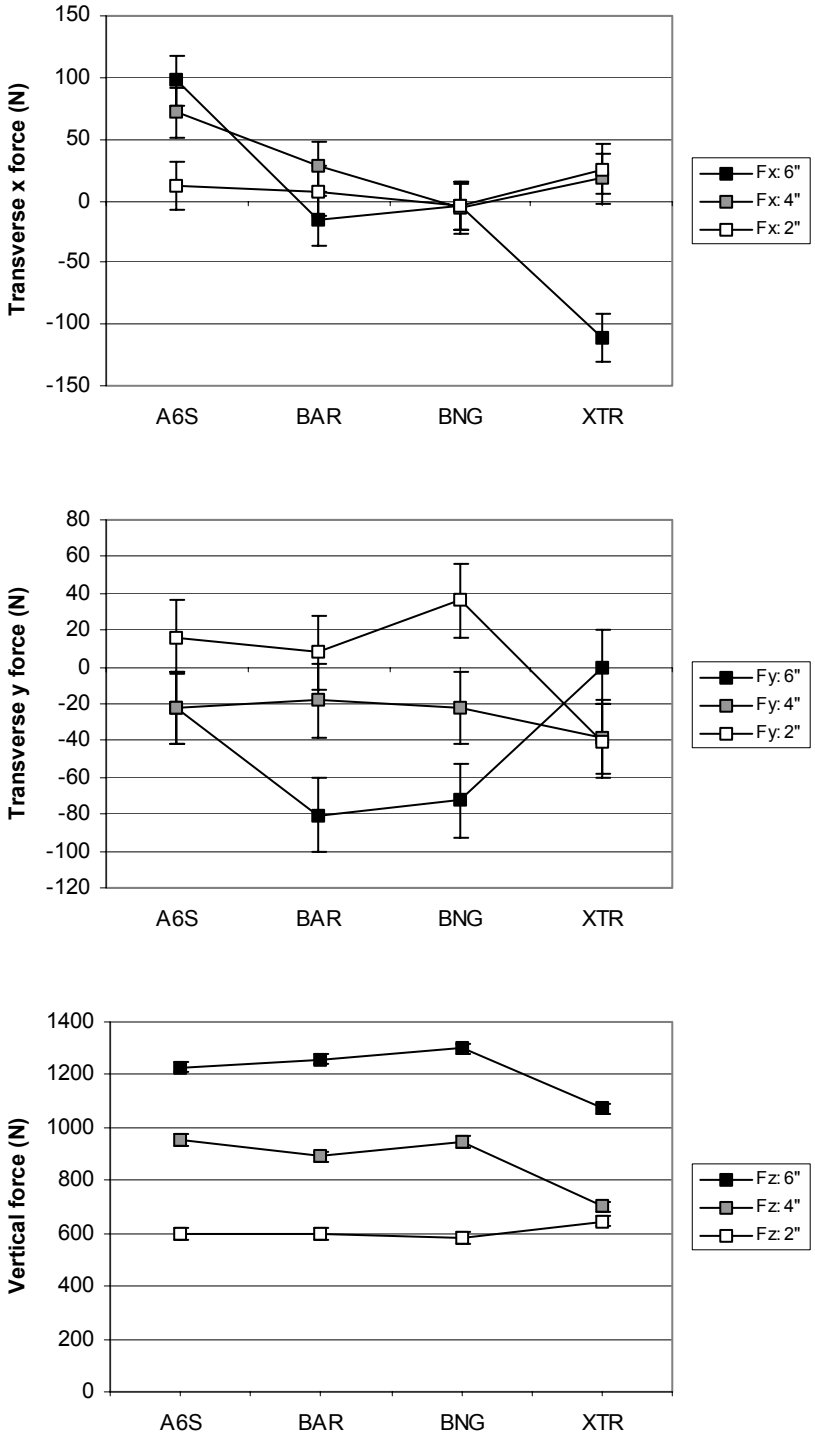

Figure 18. Mean force components in the x (top), y (middle), and z (bottom) direction for each suspension wheelchair for each curb descent.

trends between force and curb height are apparent in the upper two plots, suggesting the test pilot may have biased the results. During a curb descent a user may shift his weight and make small changes in position to maintain balance. These changes presumably result in movement of the rear wheels, which directly affect the tangential forces applied to the landing surface. Given the constraint placed on curb descents performed in this study, that the test pilot maintain a wheelie through impact, it is suspected that random adjustments made to ensure proper descent and stability affected the results. This probability is supported by the asymmetries observed in the force data, which could have led to instability following initial wheel impact.

For the plot of vertical force components, a distinct layering of the forces curve is apparent. This indicates a relationship between curb height and force. Unlike the other two force components, vertical force is dictated strictly by the mass and acceleration of the wheelchair and test pilot. The test pilot cannot alter the effective mass of himself or the wheelchair during the descent; therefore, the vertical force data is unbiased and provides the most reliable means of comparing wheelchair performance. Another equally strong reason for selecting the vertical force component to represent impact force was the relative insignificance of the tangential forces in terms of magnitude. The plots of force data shown in Figures 13-15 show the dominance of vertical force magnitude in all measurements. Inclusion of tangential forces would not have made a significant impact on overall force vector. Therefore, for this study the ideal suspension angle at impact, as governed by the vertical force, was 90º (i.e. in line with the z-axis of the force plates).

3.3.3 Guidance Tiles Testing: Vibration Dose Values

The second phase of this study, uneven surface testing, was performed to provide a baseline from which to compare wheelchair performance during curb descents. By testing the wheelchairs in their standard orientations (all four wheels on the ground), it was assumed that the suspension systems would be more capable of reducing the vibrations associated with traversing the blind guidance tiles.

Comparisons of VDV calculated from frequency-weighted seat accelerations revealed relatively no significant differences between wheelchairs. The two exceptions were the Invacare Action Xtra and the Quickie XTR. The Xtra had the lowest VDV of all wheelchairs tested; however, the value only had significance ($p = 0.0318$) in comparison to the Quickie GP. Despite the limited significance of its dose value, the Xtra offered a remarkably smooth ride, attributable to its caster wheels. Unlike the smaller, high durometer (solid) caster wheels used by the other wheelchairs, the Xtra featured 8" pneumatic caster wheels. Beyond the obvious size advantage, pneumatic caster wheels offer ideal low-level vibration reduction by their omni-directional deformability. Regardless of the approach angle, pneumatic caster wheels will deform to a given obstacle, reducing the magnitude of both the force and vibrations associated with impact.

Solid caster wheels may not adequately deform to absorb vibration energy; therefore, in order to reduce caster-based vibrations, suspension caster forks are used. Two of the wheelchairs tested in this study featured suspension caster forks, the A-6S (elastomer-based) and the Boing (spring-based). Despite the proven capability of caster suspension,[34] neither of these wheelchairs demonstrated any improvement in VDV. This suggests that either the suspension caster forks of

the A-6S and Boing are inferior to the polymer-based suspension caster forks (Frog Legs) tested by Cooper et al, or the blind guidance tiles produced unmanageable vibrations. Additional testing of various suspension caster forks on various surfaces, or under various conditions, must be done to properly address this point.

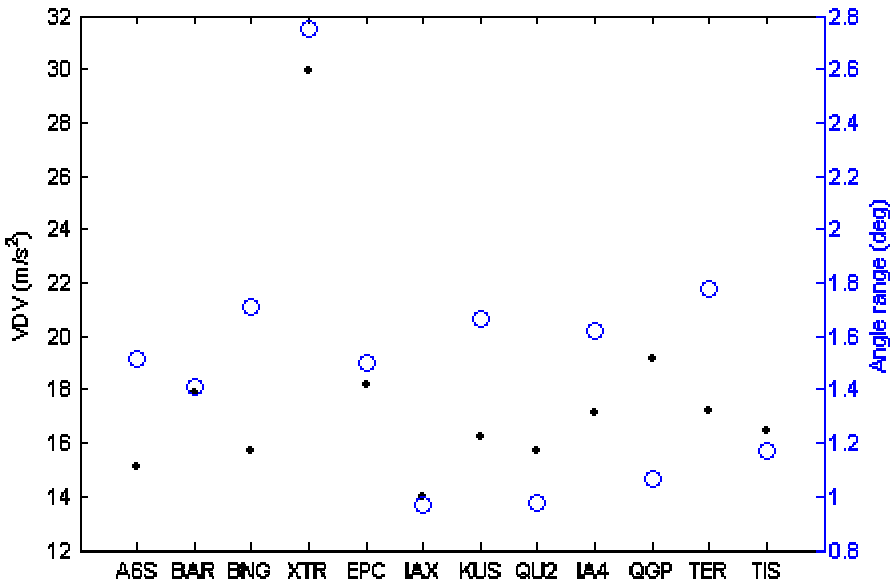

Figure 19. VDV (.) and range of angles (o) experienced during guidance tile testing.

The other, more surprising exception was the unexpectedly poor performance of the XTR. After demonstrating relatively superior vibration reduction during curb descents, the XTR had the highest VDV of all wheelchairs tested (nearly 57% higher than the second highest VDV). Analysis of Optotrak marker data revealed that the XTR experienced the largest variability in seat angle (angle range = 2.75º) throughout the testing (Figure 19). In other words, when traversing the guidance tiles, the casters of the XTR underwent the greatest amount of vertical motion. This motion is presumed to be the result of a high rearward dump angle and the weight and position of the integrated suspension. Inherent in the its structure, the cantilever frame, the

base on which the XTR was designed, has a more rearward positioned CoM than the box frame.[31] The addition of rear suspension resulted in an increased seat dump, which was caused by compression of the shock absorber under the weight of the test pilot. This further shifted the CoM of the system towards the rear wheels and increased the likelihood that the casters may lose contact with a rough surface and thus generate higher than expected seat vibrations. Overall, no trend between VDV and angle range was apparent (Figure 19); however, both of these measures may be dependent on other factors such as the CoM of the wheelchair and user.

The results from these two phases show that particular suspension designs have beneficial applications under certain testing conditions; however, no design provides ample protection from both the vibrations (shock and repetitive) and forces associated with high-load impacts and rough terrain. In this respect, considerations should be made for combining several types of suspension elements to create a more suitable system that is more capable in a variety of activities. Future research should be done to determine the limitations of each suspension element as well as the most suitable approach to integrated wheelchair suspension.

In addition, more research needs to be done on the transmission of vibrations through the casters. The second phase of the functional testing revealed that pneumatic caster wheels provide an advantage in terms of suppressing vibration transmitted through the casters and should be considered when discussing caster-based suspension. Pneumatic caster wheels are often dismissed because they require greater maintenance and, due to their size, offer limited use and maneuverability. However, the approaches to caster fork suspension, which utilize high-durometer wheels, are not optimized for all activities and may benefit from more compliant

wheels. The development of better-adapted caster suspension should be conducted along with developments in frame suspension, such that an optimized system for vibration reduction in manual wheelchairs may result. Further optimization may be obtained through a better understanding of the effects of different types of rear wheels and tires. And finally, for future testing, especially on caster-based suspension approaches, weight and weight balance must be controlled to produce more accurate results.

Consumers and clinicians should be aware of the functional capabilities of suspension manual wheelchairs to help ensure proper wheelchair selection. The results of this study are limited to specific, controlled tasks; however, the implications of these findings may be applied to other activities or obstacles and should still be considered when evaluating the appropriateness of suspension manual wheelchairs for a particular user.

3.3.4 Experimental Weight Analysis

One characteristic not considered thus far, beyond its correlation to data collected from curb descent testing, is wheelchair weight. Weight is not a controllable factor for a specific wheelchair, but nonetheless, it is important to consider how weight, particularly the additional weight imposed by the integrated suspension, affects the significance of differences in wheelchair performance. The weight of each wheelchair and the average weight for each wheelchair type are given in Table 8. When the mixed model analysis was rerun for acceleration and force data, with weight included as a random effect, changes in significance occurred. In terms of mean peak accelerations, no significant differences were found between the suspension and folding-frame wheelchairs. This suggests that if the weights of the suspension wheelchairs

were closer to those of the folding-frame wheelchairs, the suspension systems would not significantly reduce seat accelerations. In addition, significant differences were found between suspension and rigid-frame wheelchairs in terms of vertical force. This shows that the ability of the suspension systems to absorb energy compensated for the additional weight they imposed on the systems.

Table 8: Wheelchair Weights

Suspension		Folding		Rigid	
Model	Weight (lbs)	Model	Weight (lbs)	Model	Weight (lbs)
A6S	19.10	EPC	21.40	IA4	16.50
BAR	18.25	IAX	20.25	QGP	15.10
BNG	18.25	KUS	18.75	TER	13.48
XTR	17.00	QU2	19.70	TIS	13.00
Average	**18.15 ± 0.87**		**20.03 ± 1.11**		**14.52 ± 1.60**

Together these findings may be used to determine the ideal weight for a given suspension manual wheelchair such that it optimizes the ability of the system to reduce vibrations and impact force. Alternatively, this type of weight analysis can be used to help create a new, better-adapted suspension system for a given wheelchair.

3.4 CONCLUSIONS

This study found that suspension manual wheelchairs provide some level of vibration and force suppression, though the extent of their capabilities is limited by the orientation of the wheelchair during the given activity. Curb descent testing suggested that the angle at which a wheelchair impacts its landing surface can notably influence the effectiveness of the suspension in absorbing energy. As curb height increases, so too does the frame angle required to maintain stability (in a

wheelie) throughout the descent. This results in a larger suspension angle, thereby reducing the likelihood the suspension element would properly compress and dissipate the energy associated with impact. In addition, the type of suspension elements used by the system may limit the ability of the wheelchair to dissipate vibration and force generated under high-load conditions. Of all suspension wheelchairs, the Quickie XTR featured the most complex and properly oriented suspension element, consequently it demonstrated the best performance. Elastomer-based suspension systems provided good low-level vibration control; however, they became relatively ineffective in reducing higher magnitude shock vibrations and forces.

Subsequent testing on blind guidance tiles revealed no significant difference in VDV between wheelchair type, with the exceptions of the XTR and the Epic. The XTR presented the largest VDV of all wheelchairs, due to excessive caster bounce, likely caused by its rearward center of mass. On the other hand, the Epic presented the lowest VDV, probably due to its use of pneumatic caster wheels. These results, coupled with the results from curb descent testing, indicate the presence of trade-offs in performance based upon the type and integration of the suspension systems and the conditions under which they are used. Further development of suspension wheelchairs is needed to reduce current limitations and optimize their ability to protect riders from the risks associated with WBV exposure. In the meantime, wheelchair users and clinicians should consider the functionality of suspension wheelchairs when selecting a wheelchair for regular use.

4.0 SUMMARY

4.1 LIMITATIONS

The primary limitations of this research were the small sample of wheelchairs used in testing and the restrictions imposed on data collection. Fatigue testing was limited to nine wheelchairs, three from each manufacturer. More wheelchairs would have allowed for a better evaluation; however, when compared against the time and expense required for testing, their inclusion seemed unjustified. For functional testing, each model was represented by a single wheelchair in order to minimize the time necessary for testing and, consequently, the physical strain experienced by the test pilot. By limiting testing to a single wheelchair, for which only limited trials were run (three for each test condition), it is difficult to generalize the results to all wheelchairs of that model.

Wheelchair performance was defined by the results obtained from a small number of tasks. It can be argued that wheelchair users can and do avoid these activities, particularly curb descents, during daily wheelchair use. Furthermore, highly skilled riders can avoid many caster-based vibrations by simply performing a wheelie over rough surfaces. This would suggest that the guidance tile testing overestimates the level of vibration dose experienced by wheelchairs users. Therefore, the applicability of the findings may be limited to a slightly reduced group of users. Also, further testing, including tasks that better represent typical accelerations and forces

experienced by wheelchairs and their riders, may be required to better assess wheelchair suspension.

Functional testing was done using a single test pilot and a set of unmodified wheelchairs in order to eliminate the variability that would be introduced by multiple users and the countless configurations and available components for the wheelchairs. In this process, two key limitations were introduced. First, the use of a single test pilot may have biased the results towards users of his weight or skill level. In future studies, several users, representative of those who are capable of using a suspension manual wheelchair, should be used to allow the results to be generalized. Second, some of the wheelchairs featured suspension caster forks or may have been better adjusted (in standard configuration) to the user, thereby influencing wheelchair performance. The inclusion of suspension caster forks was justified by the desire to test each wheelchair in its standard configuration, regardless of components. Moreover, during fatigue testing, the suspension caster forks hurt the performance of the Colours Boing; therefore, it was necessary to determine their effect on seat accelerations during guidance tile testing. However, the effect of each suspension caster fork is unclear due to lack of data on the performance of a standard caster fork on the same wheelchair.

One final set of limitations was the lack of synchronization in data collection and the lack of video recordings of the trials. A more robust method of data acquisition, one that includes synchronized data and video, would have allowed for better identification of important events within the trials as well as a more thorough evaluation of the differences between data.

4.2 RESEARCH CONCLUSIONS

Over the course of daily activities, wheelchair users are subjected to a variety of whole-body vibrations that are suspected to cause a number of harmful physiological effects including low back pain, spinal deformities and compromised muscle strength. In efforts to prevent secondary injuries, manufacturers of manual wheelchairs have integrated suspension systems into their designs. However, based on the results obtained from this research, currently available designs do not properly address the stresses and functional conditions placed on the wheelchairs by active users. Further development of new suspension systems and methods of integration is necessary to optimize these wheelchairs for everyday use. The findings within this research should be considered for the design a system that provides adequate energy absorption for particular wheelchair orientations (i.e. during curb descents).

Another focus of future research, in addition to those previously stated, should be the tendency of manual suspension wheelchairs to absorb propulsion energy provided by the user. This type of energy absorption reduces the efficiency of the wheelchair and could lead to premature fatigue and injury in users. As a result, many wheelchair users avoid selecting suspension manual wheelchair as their everyday wheelchair, thus negating the benefits of the technology.

APPENDIX A

MATLAB programs for analysis of data collected during various height curb descents

```
% acc_scan.m
% Andrew Kwarciak

% Program calculates the minimum vertical acceleration,
% min frequency-weighted vertical acceleration, crest factor,
% and VDV of data obtained from curb descents

% Requires individual acceleration files recorded with custom
% data aquisition software written by David VanSickle

clear
clc

filename=[];
filename=input('Input filename (no extensions): ', 's')


%% ACCELEROMETER DATA-------------------------------------------------
string1=[filename, '.thr;'];
string2=['load ' string1;];
eval(string2);

% Convert voltages into accelerations (m/s^2)
    % 50.98 is the correction factor which reverts data to raw voltages
        % This step is necessary to undue alterations made by data acq
        % software, which was written for different hardware
    % 2.xxx is the zero G voltage in each direction
    % ~.200 is the sensor sensitivity (volts/G)

    string3=['acc_lat=((((' filename, '(:,1))/50.95)-2.538)/.199)*9.81;'];
    string4=['acc_fore=((((' filename, '(:,2))/50.89)-2.495)/.201)*9.81;'];
    string5=['acc_vert=((((' filename, '(:,3))/51.105)-2.537)/.200)*9.81;'];
    eval(string3)
    eval(string4)
    eval(string5)

% Find mininum peak in vertical acceleration
acc_vert_min=min(acc_vert)
min_pt=find(acc_vert==acc_vert_min);
min_pt_time=(min_pt-1)/200;

rms_vert=sqrt(mean(acc_vert.^2));
crest_fact=abs(acc_vert_min/rms_vert);

%% Activate additional code for plots that require manual peak detection
%     figure
%     plot(acc_vert)
%     title('Isolate impact minimum')
%     Pt=ginput(2)
%     Pt1=Pt(1,1)
```

```
%     Pt2=Pt(2,1)
%     acc_vert_min=min(acc_vert(Pt1:Pt2))
%     min_pt=find(acc_vert==acc_vert_min);


%% APPLY WEIGHTING FILTER-------------------------------------------
% Call frequency weighting filter
weighting_filter_design_v5;             % see next MATLAB program for details
fw_vert=filter(numd_wk,dend_wk,acc_vert);

% Find corresponding min peaks in freq-weighted vert acceleration data
min_range=(min_pt-50:min_pt+50);
fw_vert_min=min(fw_vert(min_range))
fw_min_pt=find(fw_vert==fw_vert_min);

fw_rms_vert=sqrt(mean(fw_vert.^2));
fw_crest_fact=abs(fw_vert_min/fw_rms_vert);


%% PLOT BOTH ACCELERATIONS------------------------------------------
figure
a_time=0:((length(acc_vert)/200)/(length(acc_vert)-1)):(length(acc_vert)/200);
plot(a_time,acc_vert);
plot(acc_vert);
hold on
plot(fw_vert,'r');
ylabel('Acceleration (m/s)')
title('Original Accel (blue), Freq Weighted Accel (red)')


%% DETERMINE VIBRATIONAL DOSE VALUE----------------------------------
acc_vert2=acc_vert(min_pt-100:min_pt+120); % Not used in analysis
vert4=(acc_vert2).^4;
sum_vert4=trapz(vert4);
vdv=(sum_vert4)^.25

figure
plot(acc_vert2);
title('Section of acceleration data used to calculate VDV')


%% SAVE PEAK ACCELERATION INFORMATION--------------------------------
stats=[acc_vert_min crest_fact fw_vert_min fw_crest_fact vdv];
fid=fopen('acc_info','a');
fprintf(fid,'%f\t %f\t %f\t %f\t %f\n',stats);
fclose(fid);
```

```
%function [numd_wk, dend_wk, numd_wd, dend_wd]=weighting_filter_design_v5
%Weighting based on ISO 2631-1:1997, Annex A
% Carmen DiGiovine
%numd_wk==numerator used in the filter.m function for the vertical accelration
weighting
%dend_wk==denomenator used in the filter.m function for the vertical accelration
weighting
%numd_wd==numerator used in the filter.m function for the horizontal accelration
weighting
%dend_wd==denomenator used in the filter.m function for the horizontal accelration
weighting
%
%USE WEIGHTING_FILTER_DESIGN_V4 TO EXAM PLOTS OF THE WEIGHTING FUNCTIONS
%REMOVE THE '%%' TO EXAMINE FILTERS IN LAPLACE DOMAIN AND TO PLOT
%      THE WEIGHTING FILTERS FOR THE VERTICAL ACCELERATION AND THE HORIZONTAL
ACCELERATIONS
%
%NOTE: s==p. p is used in the standards in lieu of s. s and p are just the laplace
operator
%Low pass filter
%
%                          2
%               w2
%Hl(s)=------------------------
%       2                     2
%      s  + sqrt(2)*w2*s + w2
%
%High pass filter
%                          2
%                 s
%Hh(s)=------------------------
%       2                     2
%      s  + sqrt(2)*w1*s + w1
%
%where w1=2*pi*f1
%                    w2=2*pi*f2
%
%Acceleration-Velocity Transition Filter
%            2
%                  w4           2
%        ------ * s + w4
%          w3
%Hac(s)=------------------------
%        2     w4        2
%       s  + -----*s + w4
%              Q4
%Upward step
%
%            2    w5           2
%           s  + ---- * s + w5
%                Q5
%
%Hs(s)= ------------------------------
%            2    w6          2
%           s  + ---- * s + w6
%                Q6
%
Fs=200; %Sampling Frequency
w1_k=2*pi*0.4; %High pass cut-off frequency in hertz
w1_d=w1_k;
w2_k=2*pi*100; %Low pass cut-off frequency in hertz
w2_d=w2_k;
```

```
w3_k=2*pi*12.5;
w3_d=2*pi*2.0;
w4_k=2*pi*12.5;
w4_d=2*pi*2.0;
w5_k=2*pi*2.37;
w6_k=2*pi*3.35;

Q4_k=0.63;
Q4_d=0.63;
Q5_k=0.91;
Q6_k=0.91;

%Low Pass Filter
num_l_k=w2_k^2;
den_l_k=[1 , w2_k*sqrt(2), w2_k^2];
num_l_d=w2_k^2;
den_l_d=[1 , w2_d*sqrt(2), w2_d^2];

%Transform from s-domain to z-domain using a bilinear transformation
[numd_l_k, dend_l_k]=bilinear(num_l_k, den_l_k, Fs);
[numd_l_d, dend_l_d]=bilinear(num_l_d, den_l_d, Fs);

%High Pass Filter
num_h_k=[1 0 0];
den_h_k=[1, w1_k*sqrt(2), w1_k^2];
num_h_d=[1 0 0];
den_h_d=[1, w1_d*sqrt(2), w1_d^2];
%Transform from s-domain to z-domain using a bilinear transformation
[numd_h_k, dend_h_k]=bilinear(num_h_k, den_h_k, Fs);
[numd_h_d, dend_h_d]=bilinear(num_h_d, den_h_d, Fs);

%Acceleration-Velocity Transition Filter
num_t_k=[(w4_k^2/w3_k), w4_k^2];
den_t_k=[1, w4_k/Q4_k, w4_k^2];
num_t_d=[(w4_d^2/w3_d), w4_d^2];
den_t_d=[1, w4_d/Q4_d, w4_d^2];
%Transform from s-domain to z-domain using a bilinear transformation
[numd_t_k, dend_t_k]=bilinear(num_t_k, den_t_k, Fs);
[numd_t_d, dend_t_d]=bilinear(num_t_d, den_t_d, Fs);

%Upward step Filter
num_s_k=[1, w5_k/Q5_k, w5_k^2];
den_s_k=[1, w6_k/Q6_k, w6_k^2];
%num_s_d=1;
%den_s_d=1;
%Transform from s-domain to z-domain using a bilinear transformation
[numd_s_k, dend_s_k]=bilinear(num_s_k, den_s_k, Fs);
%NOTE:  The upward step filter for the horizontal direction is unity so
%                   we don't need to worry about it.

%Combine Filters in s-domain (aka laplace)
num_h_l_k=conv(num_l_k, num_h_k);
num_h_l_d=conv(num_l_d, num_h_d);
den_h_l_k=conv(den_l_k, den_h_k);
den_h_l_d=conv(den_l_d, den_h_d);
num_t_s_k=conv(num_t_k, num_s_k);
den_t_s_k=conv(den_t_k, den_s_k);
num_wk=conv(num_h_l_k, num_t_s_k);
num_wd=conv(num_h_l_d, num_t_d);
den_wk=conv(den_h_l_k, den_t_s_k);
den_wd=conv(den_h_l_d, den_t_d);

%[numd_w_k, dend_w_k]=bilinear(num_w_k, den_w_k, Fs);
```

```
%[numd_w_d, dend_w_d]=bilinear(num_w_d, den_w_d, Fs);

%Combine Filters in the z-domain
       %Weightings for vertical accelerations
numd_h_l_k=conv(numd_l_k, numd_h_k);
dend_h_l_k=conv(dend_l_k, dend_h_k);
numd_t_s_k=conv(numd_t_k, numd_s_k);
dend_t_s_k=conv(dend_t_k, dend_s_k);
numd_wk=conv(numd_h_l_k, numd_t_s_k);
dend_wk=conv(dend_h_l_k, dend_t_s_k);
       %Weightings for horizontal accelerations (fore-to-aft & lateral)
numd_h_l_d=conv(numd_l_d, numd_h_d);
dend_h_l_d=conv(dend_l_d, dend_h_d);
numd_wd=conv(numd_h_l_d, numd_t_d);
dend_wd=conv(dend_h_l_d, dend_t_d);
```

```
% force_scan.m
% Andrew Kwarciak - incorporates code written by Song Feng Guo

% Calculates the time (data point) and magnitude of the initial
% spike and maximum force recorded from each force plate during
% curb descents.

% Requires stream of force plate data collected using custom
% LabVIEW program

clear
clc

filename=[];
filename=input('Input filename (no extensions): ', 's')

stringL=['load ',filename];
eval(stringL)

stringA=['a=',filename,';'];
eval(stringA);

% Separates stream of force plate data into 6 distinct forces
j=1;
k=0;
i=1;

while i<=51800
   if a(i)==4 & a(i+1)==170

      irfx(j)=a(i+2);
      irfy(j)=a(i+3);
      irfz(j)=a(i+4);
      ilfx(j)=a(i+8);
      ilfy(j)=a(i+9);
      ilfz(j)=a(i+10);

      j=j+1;
      i=i+26;
   else
     i=i+1;
   end
end

% Trim data to eliminate bad points
figure
plot(irfz,'r')
hold on
plot(ilfz)
title('Choose baseline (1 point) and range of solid force plate data (2 points)')

P=ginput(3)
P1=floor(P(1,1));
P2=floor(P(2,1));
P3=ceil(P(3,1));

    % Using baseline point - convert force data to Newtons (using calibration.m)
    rfx=(irfx-irfx(P1))*5.9598;
    lfx=(ilfx-ilfx(P1))*5.9598;
    rfy=(irfy-irfy(P1))*6.0518;
    lfy=(ilfy-ilfy(P1))*6.0518;
    rfz=(irfz-irfz(P1))*23.6239;
    lfz=(ilfz-ilfz(P1))*23.6239;
```

```
% Define trimmed data
trfx=rfx(P2:P3);
tlfx=lfx(P2:P3);
trfy=rfy(P2:P3);
tlfy=lfy(P2:P3);
trfz=rfz(P2:P3);
tlfz=lfz(P2:P3);

% Find values and points for the initial spike and the maximum force
% Start with the right side
figure
plot(trfz,'r')
title('Surround both the initial spike and maximum spike')
R=ginput(4);
R1=floor(R(1,1));
R2=ceil(R(2,1));
R3=floor(R(3,1));
R4=ceil(R(4,1));

rspike=max(trfz(R1:R2))         % Value of initial spike
trfz_12=trfz(R1:R2);
R5=find(trfz_12==rspike);
rspike_pt=(P2+R1+R5(1)-2)       % Point of initial spike

rmaxforce=max(trfz(R3:R4))      % Value of max force
trfz_34=trfz(R3:R4);
R6=find(trfz_34==rmaxforce);
rmaxforce_pt=(P2+R3+R6(1)-1)    % Point of max force

% Repeat steps for left side
figure
plot(tlfz)
title('Surround both the initial spike and maximum spike')
L=ginput(4);
L1=floor(L(1,1));
L2=ceil(L(2,1));
L3=floor(L(3,1));
L4=ceil(L(4,1));

lspike=max(tlfz(L1:L2))         % Value of initial spike
tlfz_12=tlfz(L1:L2);
L5=find(tlfz_12==lspike);
lspike_pt=(P2+L1+L5(1)-2)       % Point of initial spike

lmaxforce=max(tlfz(L3:L4))      % Value of max force
tlfz_34=tlfz(L3:L4);
L6=find(tlfz_34==lmaxforce);
lmaxforce_pt=(P2+L3+L6(1)-1)    % Point of max force


%% SET TIMESCALE-------------------------------------------------
f_time=0:((length(rfz)/400)/(length(rfz)-1)):(length(rfz)/400);


%% SAVE PEAK ACCELERATION INFORMATION---------------------------------
forces=[rspike   rspike_pt   rmaxforce   rmaxforce_pt   lspike   lspike_pt   lmaxforce
lmaxforce_pt];
fid=fopen('force_info','a');
fprintf(fid,'%f\t %f\t %f\t %f\t %f\t %f\t %f\t %f\n',forces);
fclose(fid);
```

```
% force_scan3.m
% Andrew Kwarciak - modification of force_scan.m

% Produces converted and trimmed forces components for
% plotting and presentation in paper - used only for suspension
% wheelchairs

clear
clc

filename=[];
filename=input('Input filename (no extensions): ', 's')

stringL=['load ',filename];
eval(stringL)

stringA=['a=',filename,';'];
eval(stringA);

% Separates stream of force plate data into 6 distinct forces
j=1;
k=0;
i=1;

while i<=51800
   if a(i)==4 & a(i+1)==170

      irfx(j)=a(i+2);
      irfy(j)=a(i+3);
      irfz(j)=a(i+4);
      ilfx(j)=a(i+8);
      ilfy(j)=a(i+9);
      ilfz(j)=a(i+10);

      j=j+1;
      i=i+26;
   else
     i=i+1;
   end
end

% Trim data to eliminate bad points
figure
plot(irfz,'r')
hold on
plot(ilfz,'b')
title('Choose baseline (1 point) and range of solid force plate data (2 points)')

P=ginput(3)
P1=floor(P(1,1));
P2=floor(P(2,1));
P3=ceil(P(3,1));

    % Using baseline point - convert force data to Newtons (using calibration.m)
    rfx=(irfx-irfx(P1))*5.9598;
    lfx=(ilfx-ilfx(P1))*5.9598;
    rfy=(irfy-irfy(P1))*6.0518;
    lfy=(ilfy-ilfy(P1))*6.0518;
    rfz=(irfz-irfz(P1))*23.6239;
    lfz=(ilfz-ilfz(P1))*23.6239;

trfx=rfx(P2:P3);
tlfx=lfx(P2:P3);
```

```
trfy=rfy(P2:P3);
tlfy=lfy(P2:P3);
trfz=rfz(P2:P3);
tlfz=lfz(P2:P3);

figure
plot(trfz,'r')
hold on
plot(tlfz)
title('Surround the maximum spike')
R=ginput(2);
R1=floor(R(1,1));
R2=ceil(R(2,1));

rspike=max(trfz(R1:R2));
lspike=max(tlfz(R1:R2));
R3=find(trfz==rspike);
R4=find(tlfz==lspike);

pts=[R3(1) R4(1)];
pt=max(pts);

R5=(P2+pt(1)-1);

frfx=rfx(R5-50:R5+99);
flfx=lfx(R5-50:R5+99);
frfy=rfy(R5-50:R5+99);
flfy=lfy(R5-50:R5+99);
frfz=rfz(R5-50:R5+99);
flfz=lfz(R5-50:R5+99);

figure
plot(frfx,'r')
hold on
plot(frfy,'r')
hold on
plot(frfz,'r')
hold on
plot(flfx,'b')
hold on
plot(flfy,'b')
hold on
plot(flfz,'b')


%% SAVE PEAK ACCELERATION INFORMATION--------------------------------
forces=[frfx' frfy' frfz' flfx' flfy' flfz'];
fid=fopen('forceplots_tis6in','a');     % line changes to open new file for each chair
fprintf(fid,'%f\t %f\t %f\t %f\t %f\t %f\t',forces);
fclose(fid);
```

```
% force_scan4.m
% Andrew Kwarciak - modifcation of force_scan.m

% Produces converted force components for both force plates
% Requires stream of force plate data collected using custom
% LabVIEW program

clear
clc

filename=[];
filename=input('Input filename (no extensions): ', 's')

stringL=['load ',filename];
eval(stringL)

stringA=['a=',filename,';'];
eval(stringA);

% Separates stream of force plate data into 6 distinct forces
j=1;
k=0;
i=1;

while i<=51800
   if a(i)==4 & a(i+1)==170

      irfx(j)=a(i+2);
      irfy(j)=a(i+3);
      irfz(j)=a(i+4);
      ilfx(j)=a(i+8);
      ilfy(j)=a(i+9);
      ilfz(j)=a(i+10);

      j=j+1;
      i=i+26;
   else
     i=i+1;
   end
end

% Trim data to eliminate bad points
plot(irfz,'r')
hold on
plot(ilfz,'b')
title('Choose baseline (1 point) and range of solid force plate data (2 points)')

P=ginput(3)
P1=floor(P(1,1));
P2=floor(P(2,1));
P3=ceil(P(3,1));

    % Using baseline point - convert force data to Newtons (using calibration.m)
    rfx=(irfx-irfx(P1))*5.9598;
    lfx=(ilfx-ilfx(P1))*5.9598;
    rfy=(irfy-irfy(P1))*6.0518;
    lfy=(ilfy-ilfy(P1))*6.0518;
    rfz=(irfz-irfz(P1))*23.6239;
    lfz=(ilfz-ilfz(P1))*23.6239;

trfx=rfx(P2:P3);
tlfx=lfx(P2:P3);
trfy=rfy(P2:P3);
```

```
tlfy=lfy(P2:P3);
trfz=rfz(P2:P3);
tlfz=lfz(P2:P3);

% Find values and points for the initial spike
% Start with the right side
rspike_z=max(trfz);                 % Value of initial spike
R3=find(trfz==rspike_z);
rspike_pt=(P2+R3(1)-1);             % Point of initial spike

rspike_x=trfx(R3(1));
rspike_y=trfy(R3(1));


% Repeat steps for left side
lspike_z=max(tlfz);                 % Value of initial spike
L3=find(tlfz==lspike_z);
lspike_pt=(P2+L3(1)-1);             % Point of initial spike

lspike_x=tlfx(L3(1));
lspike_y=tlfy(L3(1));


%% SAVE PEAK ACCELERATION INFORMATION--------------------------------
forces=[rspike_x rspike_y rspike_z lspike_x lspike_y lspike_z (rspike_pt-lspike_pt)];
fid=fopen('force_scan4','a');
fprintf(fid,'%f\t %f\t %f\t %f\t %f\t %f\t %f\n',forces);
fclose(fid);
```

```
% optotracesX.m
% Andrew Kwarciak

% Trims Optotrak marker data and calculates the minimum
% and maximum angle of the wheelchair throughout curb
% descent as well as the angle of the wheelchair at impact

clear
clc

filename=[];
filename=input('Input filename (no extensions): ', 's')

string10=[filename(1:3),filename(8)];
string11=['load ' string10 '.txt'];
eval(string11)


%% OPTOTRAK MARKER 1: AXLE--------------------------------------
string12=['mark1_x = ' string10, '(:,2);'];
eval(string12)
string13=['mark1_z = ' string10, '(:,4);'];
eval(string13)

% Trim data to exclude lost marker points near end of trial
mark1_x_min_pt=find(mark1_x==min(mark1_x));
mark1_z_min_pt=find(mark1_z==min(mark1_z));
mark1_x_min_pt=mark1_x_min_pt(1);
mark1_z_min_pt=mark1_z_min_pt(1);

mark1_x_min=min(mark1_x);
mark1_z_min=min(mark1_z);

if mark1_x_min < -2000
    mark1_x=mark1_x(1:(mark1_x_min_pt-1));
    mark1_z=mark1_z(1:(mark1_z_min_pt-1));
else
    mark1_x=mark1_x;
    mark1_z=mark1_z;
end

% Further trim data and locate the point of impact
figure
plot(mark1_z,'k');
title('Choose 2 points that surround initial max (impact)')
M=ginput(2);
M1=floor(M(1,1));
M2=ceil(M(2,1));

M_subset=mark1_z(M1:M2);
M3=find(M_subset==max(M_subset));
opto_hit_pt=(M1+M3(1)-1)
opto_hit_time=((opto_hit_pt-1)/300);

% Trim marker data to a few points beyond impact
mark1_x=mark1_x(1:(opto_hit_pt+20));
mark1_z=mark1_z(1:(opto_hit_pt+20));


% %% OPTOTRAK MARKER 2: CLOSEST TO REAR WHEEL--------------------
string14=['mark2_x = ', string10, '(:,5);'];
eval(string14)
string15=['mark2_z = ', string10, '(:,7);'];
```

```
eval(string15)

% Trim marker data to a few points beyond impact
mark2_x=mark2_x(1:(opto_hit_pt+20));
mark2_z=mark2_z(1:(opto_hit_pt+20));


% %% OPTOTRAK MARKER 3: MIDDLE-----------------------------------
string16=['mark3_x = ', string10, '(:,8);'];
eval(string16)
string17=['mark3_z = ', string10, '(:,10);'];
eval(string17)

% Trim marker data to a few points beyond impact
mark3_x=mark3_x(1:(opto_hit_pt+20));
mark3_z=mark3_z(1:(opto_hit_pt+20));


% %% OPTOTRAK MARKER 4: CLOSEST TO FOOTRESTS-------------------
string18=['mark4_x = ', string10, '(:,11);'];
eval(string18)
string19=['mark4_z = ', string10, '(:,13);'];
eval(string19)

% Trim marker data to a few points beyond impact
mark4_x=mark4_x(1:(opto_hit_pt+20));
mark4_z=mark4_z(1:(opto_hit_pt+20));


%% SET BASELINE-----------------------------------------
string20=['floor1_x=' ,string10, '(:,14);'];
eval(string20)
string21=['floor1_z=' ,string10, '(:,16);'];
eval(string21)
string22=['floor2_x=' ,string10, '(:,17);'];
eval(string22)
string23=['floor2_z=' ,string10, '(:,19);'];
eval(string23)

floor1_x=floor1_x(1:(opto_hit_pt+20));
floor1_z=floor1_z(1:(opto_hit_pt+20));
floor2_x=floor2_x(1:(opto_hit_pt+20));
floor2_z=floor2_z(1:(opto_hit_pt+20));

% figure                    % Uncomment for plot marker positions
% plot(mark1_x,-mark1_z,'k');
% hold on
% plot(mark2_x,-mark2_z,'c');
% hold on
% plot(mark3_x,-mark3_z,'g');
% hold on
% plot(mark4_x,-mark4_z,'r');
% ylabel('Height (mm)')
% xlabel('Position')


%% FIND FRAME ANGLE THROUGHOUT TRIAL
for i=1:opto_hit_pt+20
    A(i,:)=[mark4_x(i),-mark4_z(i)]-[mark3_x(i),-mark3_z(i)];
    B(i,:)=[floor2_x(i),-floor2_z(i)]-[floor1_x(i),-floor1_z(i)];
    C(i)=dot(A(i,:),B(i,:));

    % Take the hypotenuse between two points
```

```
    mag_A(i)=sqrt((A(i,1))^2+(A(i,2))^2);
    mag_B(i)=sqrt((B(i,1))^2+(B(i,2))^2);

    % Find angle by dividing inverse cosine of angle by
    % magnitude of two vectors forming angle
    angle(i,1)=(360/(2*pi))*acos(C(i)/((mag_A(i))*(mag_B(i))));

    i=i+1;
end

figure
plot((-mark1_z/25.4)-11.25,'k');
ax1=gca;
xlabel('Data point')
ylabel('Axle height (in)')
set(ax1,'YColor','k');
ax2                                                                                =
axes('Position',get(ax1,'Position'),'XAxisLocation','top','YAxisLocation','right','Col
or','none','XColor','k','YColor','b');
hold on
plot(angle,'b:')
ylabel('Angle (deg)')

angles=[max(angle) min(angle) hit_angle];
fid=fopen('curb_angles','a');
fprintf(fid,'%f\t %f\t %f\n',angles);
fclose(fid);
```

APPENDIX B

MATLAB programs for analysis of data collected during blind guidance tile testing

```
% acc_scan_dimple2.m
% Andrew Kwarciak - modification of acc_scan.m

% Program calculates the root mean square, the positive and
% negative crest factor and the VDV of acceleration data
% obtained while traversing blind guidance tiles

% Requires individual acceleration files recorded with custom
% data aquisition software written by David VanSickle

clear
clc

filename=[];
filename=input('Input filename (no extensions): ', 's')

string1=[filename, '.thr;'];
string2=['load ' string1;];
eval(string2);

% Convert voltages into accelerations (m/s^2)
    % 50.98 is the correction factor which reverts data to raw voltages
        % This step is necessary to undue alterations made by data acq
        % software, which was written for different hardware
    % 2.xxx is the zero G voltage in each direction
    % ~.200 is the sensor sensitivity (volts/G)

    string3=['acc_lat=((((' filename, '(:,1))/50.95)-2.538)/.199)*9.81;'];
    string4=['acc_fore=((((' filename, '(:,2))/50.89)-2.495)/.201)*9.81;'];
    string5=['acc_vert=((((' filename, '(:,3))/51.105)-2.537)/.200)*9.81;'];
    eval(string3)
    eval(string4)
    eval(string5)

% Identify marker points and magnitudes
string6=['index_marker=find(' filename, '(:,12)==1);']
eval(string6);

% Use markers to trim data
acc_vert=acc_vert(index_marker(1):index_marker(1)+680);
acc_vert=acc_vert(41:length(acc_vert)-41);           % All data trimmed to 600 pts (3
sec)

figure
plot(acc_vert);

% Find mininum peak in vertical acceleration
acc_vert_min=min(acc_vert)
min_pt=find(acc_vert==acc_vert_min);
min_pt_time=(min_pt-1)/200;
```

```
rms_vert=sqrt(mean(acc_vert.^2));
crest_fact=abs(acc_vert_min/rms_vert);

%% ESTIMATE THE PSD
% After inspecting results, PSD was not included analysis
figure
psd(acc_vert,[],200);
% pwelch(acc_vert,[],[],[],200)
str=['title(''PSD Estimate of ' filename(1:3),filename(8), ''')']
eval(str)


%% APPLY WEIGHTING FILTER-------------------------------------------
weighting_filter_design_v5;
fw_vert=filter(numd_wk,dend_wk,acc_vert);

% Find freq weighted min, rms, and crest factor
fw_vert_min=min(fw_vert);
fw_vert_max=max(fw_vert);
fw_min_pt=find(fw_vert==fw_vert_min);

fw_rms_vert=sqrt(mean(fw_vert.^2));
fw_neg_crest_fact=abs(fw_vert_min/fw_rms_vert);
fw_pos_crest_fact=abs(fw_vert_max/fw_rms_vert);


%% DETERMINE VIBRATIONAL DOSE VALUE---------------------------------
vert4=(fw_vert).^4;
sum_vert4=trapz(vert4);
vdv=(sum_vert4)^.25


%% SAVE ACCELERATION INFORMATION-----------------------------------
d_stats=[rms_vert fw_neg_crest_fact fw_pos_crest_fact vdv];
fid=fopen('dimple_info','a');
fprintf(fid,'%f\t %f\t %f\t %f\n',d_stats);
fclose(fid);
```

```
% optotracesY.m
% Andrew Kwarciak - modification of optotracesX.m

% Trims Optotrak marker data and calculates the minimum,
% maximum and mean (plus st dev) angle experienced while
% traversing blind guidance tiles

% Requires acceptable range of position data, when all four
% markers are in view of the camera, for proper analysis

clear

filename=input('Input filename (no extensions): ', 's')
string1=['load ' filename '.txt'];
eval(string1);
range=input('Enter (as a vector) acceptable range of Optotrak data: ');


%% OPTOTRAK MARKER 1: AXLE-------------------------------------
string12=['mark1_x = ' filename, '(:,2);'];
eval(string12)
string13=['mark1_z = ' filename, '(:,4);'];
eval(string13)

% Trim data to selected range
mark1_x=mark1_x(range(1):range(2));
mark1_z=mark1_z(range(1):range(2));


% %% OPTOTRAK MARKER 2: CLOSEST TO REAR WHEEL--------------------
string14=['mark2_x = ', filename, '(:,5);'];
eval(string14)
string15=['mark2_z = ', filename, '(:,7);'];
eval(string15)

% Trim marker data to a few points beyond impact
mark2_x=mark2_x(range(1):range(2));
mark2_z=mark2_z(range(1):range(2));


% %% OPTOTRAK MARKER 3: MIDDLE-----------------------------------
string16=['mark3_x = ', filename, '(:,8);'];
eval(string16)
string17=['mark3_z = ', filename, '(:,10);'];
eval(string17)

% Trim marker data to a few points beyond impact
mark3_x=mark3_x(range(1):range(2));
mark3_z=mark3_z(range(1):range(2));


% %% OPTOTRAK MARKER 4: CLOSEST TO FOOTRESTS-------------------
string18=['mark4_x = ', filename, '(:,11);'];
eval(string18)
string19=['mark4_z = ', filename, '(:,13);'];
eval(string19)

% Trim marker data to a few points beyond impact
mark4_x=mark4_x(range(1):range(2));
mark4_z=mark4_z(range(1):range(2));


%% SET BASELINE-----------------------------------------------
```

```
base=(min(-mark1_z))-10;
baseline=base*ones(1,2000);


%% FIND FRAME ANGLE THROUGHOUT TRIAL----------------------------
for i=1:length(mark1_x)
    A(i,:)=[mark4_x(i),-mark4_z(i)]-[mark2_x(i),-mark2_z(i)];
    B(i,:)=[i+1,baseline(i+1)]-[i,baseline(i)];     % Creates fake floor vector
    C(i)=dot(A(i,:),B(i,:));

    % Take the hypotenuse between two points
    mag_A(i)=sqrt((A(i,1))^2+(A(i,2))^2);
    mag_B(i)=sqrt((B(i,1))^2+(B(i,2))^2);

    % Find angle by dividing inverse cosine of angle by
    % magnitude of two vectors forming angle
    angle(i,1)=(360/(2*pi))*acos(C(i)/((mag_A(i))*(mag_B(i))));
end

% Plot axle position against frame angle
figure
plot(-mark1_z,'k');
ax1=gca;
xlabel('Data point')
ylabel('Axle height')
set(ax1,'YColor','k');
ax2                                                                                    =
axes('Position',get(ax1,'Position'),'XAxisLocation','top','YAxisLocation','right','Col
or','none','XColor','k','YColor','b');
hold on
plot(angle,'b')
ylabel('Angle (deg)')

angles=[max(angle) min(angle) mean(angle) std(angle)];
fid=fopen('angleinfo','a');
fprintf(fid,'%f\t %f\t %f\t %f\n',angles);
fclose(fid);
```

BIBLIOGRAPHY

1. Griffin MJ. Handbook of human vibration. San Diego: Academic Press; 1990.

2. Wilder DG, Pope MH. Epidemiological and aetiological aspects of low back pain in vibration environments – an update. Clin Biomech 1996;11(2):61-73.

3. Pope MH, Wilder DG, Magnusson ML. A review of studies on seated whole-body vibration and low back pain. In Proc Inst Mech Eng, Part H 1999;213:435-46.

4. Bovenzi M, Hulshof CTJ. An updated review of epidemiologic studies on the relationship between exposure to whole-body vibrations and low back pain (1986-1997). Int Arch Occup Environ Health 1999;72:351-65.

5. Lings S, Leboeuf-Yde C. Whole-body vibration and low back pain: a systematic, critical review of the epidemiological literature 1992-1999. Int Arch Occup Environ Health 2000;73:290-97.

6. El-Khatib A, Guillon F. Lumbar intradiscal pressure and whole-body vibration – first results. Clin Biomech 2001;16(Supplement No 1):S127-34.

7. Matsumoto Y, Griffin MJ. Effect of phase on human response to vertical whole-body vibration and shock – analytical investigation. J Sound Vibration 2002;250(5):813-34.

8. Pope MH, Goh KL, Magnusson ML. Spine Ergonomics. Ann Rev Biomed Eng 2002;4:49-68.

9. Blüthner R, Seidel H, Hinz B. Myoelectric response of back muscles to vertical random whole-body vibration with different magnitudes at different postures. J Sound Vibration 2002;253(1):37-56.

10. Matsumoto Y, Griffin MJ. Effect of muscle tension on non-linearities in the apparent masses of seated subjects exposed to vertical whole-body vibration. J Sound Vibration 2002;253(1):77-92.

11. Hinz B, Seidel H, Menzel G, Blüthner R. Effects related to random whole-body vibration and posture on a suspended seat with and without backrest. J Sound Vibration 2002;253(1):265-82.

12. Seidel H, Griffin MJ. Modeling the response of the spinal system to whole-body vibration and repeated shock. Clin Biomech 2001;16(Supplement No 1):S3-7.

13. Matsumoto Y, Griffin MJ. Modelling the dynamic mechanisms associated with the principal resonance of the seated human body. Clin Biomech 2001;16(Supplement No 1):S31-44.

14. Matsumoto Y, Griffin MJ. Non-linear characterists in the dynamic responses of seated subjects exposed to vertical whole-body vibration. J Biomech Eng 2002;124:527-32.

15. Nawayseh N, Griffin MJ. Non-linear dual-axis biodynamic response to vertical whole-body vibration. J Sound Vibration 2003;268:503-23.

16. Hoover AE, Cooper RA, Dan D, Dvorsnak M, Cooper R, Fitzgerald SG, Boninger ML. Comparing driving habits of wheelchair users: manual versus power. Proceedings of the RESNA 26th International Conference on Technology & Disability; 2003 June 19-23; Atlanta (GA). Arlington (VA): RESNA Press; 2003:CD-ROM.

17. VanSickle DP, Cooper RA, Boninger ML. Road loads acting on manual wheelchairs. IEEE Trans Rehab Eng 2000;8(3):371-84.

18. Dupuis H, Hartung E, Haverkamp M. Acute effects of transient vertical whole-body vibrations. Int Arch of Occup Environ Health 1991;63:261-5.

19. VanSickle DP, Cooper RA, Boninger ML, DiGiovine CP. Analysis of vibrations induced during wheelchair propulsion. J Rehabil Res Dev 2001;38:409-21.

20. International Organization for Standardization, Geneva, Switzerland, ISO 2631-1, 1997.

21. Tai C, Liu D, Cooper RA, DiGiovine MM, Boninger ML. Analysis of vibrations during manual wheelchair use. Saudi J Disabil Rehab 1998;4(3):186-91.

22. DiGiovine CP, Cooper RA, Fitzgerald SG, Boninger ML, Wolf EJ, Guo S. Whole-body vibration during manual wheelchair propulsion with selected seat cushions and back supports. IEEE Trans Neural Systems Rehab Eng 2003;11(3):311-22.

23. Harris CM. Shock and vibration handbook. 3rd ed. New York: McGraw-Hill; 1988.

24. American National Standards Institute. American national standard for wheelchairs–volume 1: requirements and test methods for wheelchairs (including scooters). New York: American National Standards Institute; 1998.

25. Cooper RA, Robertson RN, Lawrence B, Heil T, Albright SJ, VanSickle DP et al. Life-cycle analysis of depot versus rehabilitation manual wheelchairs. J Rehabil Res Dev 1996;33:45-55.

26. Cooper RA, Boninger ML, Rentschler AJ. Evaluation of selected ultralight manual wheelchairs using ANSI/RESNA standards. Arch Phys Med Rehabil 1999;80:462-7.

27. Fitzgerald SG, Cooper RA, Boninger ML, Rentschler AJ. Comparison of fatigue life for three types of manual wheelchairs. Arch Phys Med Rehabil 2001;82:1-6.

28. Cooper RA, Gonzalez J, Lawrence B, Rentschler A, Boninger ML, VanSickle DP. Performance of selected lightweight wheelchairs on ANSI/RESNA tests. Arch Phys Med Rehabil 1997;78:1138-44.

29. International Standards Organization (ISO), Committee Draft ISO/CD 7176-8(E). Wheelchairs – part 8: requirements and test methods for static, impact, and fatigue strength. Zurich, Switzerland: Technical Committee 173, Subcommittee 1, N 200; December 1994.

30. Green SB and Salkind NJ. Using SPSS for Windows and Macintosh: Analyzing and Understanding Data. 3rd ed. Upper Saddle River (NJ): Prentice Hall; 2003.

31. Cooper RA. Wheelchair Selection and Configuration. New York: Demos Medical Publishing; 1998.

32. Lancaster JF. Metallurgy of Welding. 5th ed. New York: Chapman & Hall; 1993.

33. Fitzgerald SG, Yoest LM, Cooper RA, Downs F. Comparison of laboratory and actual fatigue life for three types of manual wheelchairs. Proceedings of the RESNA 2001 Annual Conference: 2001 June 22-25; Reno (NV). Arlington (VA): RESNA Press; 2001. p 352-4.

34. Cooper RA, Wolf E, Fitzgerald SG, Boninger ML, Ulerich R, Ammer WA. Seat and footrest shocks and vibrations in manual wheelchairs with and without suspension. Arch Phys Med Rehab 2003;84:96-102.

35. Kitazaki S, Griffin MJ. Resonance behaviour of the seated human body and effect on posture. J Biomech 1998;31:143-9.

36. Kwarciak AM, Cooper RA, Wolf EJ. Effectiveness of rear suspension in reducing shock exposure to manual wheelchair users during curb descents. Proceedings of the RESNA 25th International Conference; 2002 June 27-July 1; Minneapolis (MN). Arlington (VA): RESNA Press; 2002. p 365-7.

37. Wolf E, Cooper RA, Kwarciak A. Analysis of whole-body vibrations of suspension manual wheelchairs: utilization of the absorbed power method. Proceedings of the RESNA 25th International Conference; 2002 June 27-July 1; Minneapolis (MN). Arlington (VA): RESNA Press; 2002. p 303-5.

38. Hostens I, Papaioannou, Spaepen A, Ramon H. A study of vibration characteristics on a luxury wheelchair and a new prototype wheelchair. J Sound Vibration 2003;266:443-452.

39. Corfman TA, Cooper RA, Fitzgerald SG, Cooper R. A video-based analysis of "tips and falls" during electric powered wheelchair driving, Arch Phys Med Rehab 2003;84(12):1797-1802.

40. Lundström R, Holmlund P, Lindberg L. Absorption of energy during vertical whole-body vibration exposure. J Biomech 1998;31:317-326.

Suppliers

a. Invacare Corp, 1 Invacare Way, PO Box 4028, Elyria, OH 44036-2125.

b. Colours by Permobil, 1591 S Sinclair Street, Anaheim, CA 92806.

c. Sunrise Medical Inc, 2382 Faraday Avenue, Suite 200, Carlsbad, CA 92008-7220.

d. SPSS Inc, 233 S Wacker Drive, 11th Floor, Chicago, IL 60606.

e. Everest & Jennings, 1100 Corporate Square Drive, St. Louis, MO 63132.

f. Kuschall of America, 708 Via Alondra, Camarillo, CA 93012.

g. TiSport, 1426 E Third Avenue, Kennewick, Washington 99337

h. Crossbow Technology, 41 E Daggett Drive, San Jose, CA 95134.

i. Northern Digital Inc, 103 Randall Drive, Waterloo, Ontario, Canada N2V 1C5

j. National Instruments Corp, 11500 N Mopac Expressway, Austin, TX 78759-3504.

k. The Math Works Inc, 3 Apple Hill Drive, Natick, MA 01760-2098.

l. SAS Institute Inc, SAS Campus Drive, Cary, NC 27513.